

Finding groups of cross-correlated features in bi-view data

Miheer Dewaskar*

MIHEER.DEWASKAR@DUKE.EDU

*Department of Statistical Science
Duke University
Durham, NC 27708-0251, USA*

John Palowitch

JOHNPALOWITCH@GMAIL.COM

*Google Research
California, USA*

Mark He

TH2953@CUMC.COLUMBIA.EDU

*Columbia University Mailman School of Public Health
722 West 168th St., NY 10032, USA*

Michael I. Love

MILOVE@EMAIL.UNC.EDU

*Department of Biostatistics and Department of Genetics
University of North Carolina at Chapel Hill
Chapel Hill, NC 27599-7400, USA*

Andrew B. Nobel

NOBEL@EMAIL.UNC.EDU

*Department of Statistics and Operations Research and Department of Biostatistics
University of North Carolina at Chapel Hill
Chapel Hill, NC 27599-3260, USA*

Editor:

Abstract

Data sets in which measurements of two (or more) types are obtained from a common set of samples arise in many scientific applications. A common problem in the exploratory analysis of such data is to identify groups of features of different data types that are strongly associated. A bimodule is a pair (A, B) of feature sets from two data types such that the aggregate cross-correlation between the features in A and those in B is large. A bimodule (A, B) is *stable* if A coincides with the set of features that have significant aggregate correlation with the features in B , and vice-versa. In this paper we propose and investigate an iterative testing-based procedure (BSP) to identify stable bimodules in bi-view data. We carry out a thorough simulation study to assess the performance of BSP, and present an extended application to the problem of expression quantitative trait loci (eQTL) analysis using recent data from the GTEx project. In addition, we apply BSP to climatology data to identify regions in North America where annual temperature variation affects precipitation.

Keywords: cross-correlation network, iterative testing, permutation distribution, eQTL analysis, temperature and precipitation correlation.

*. corresponding author

1. Introduction

The increasing development and application of measurement technologies in fields such as genomics and neuroscience means that researchers are often faced with the task of analyzing data sets that contain different measurements derived from a common set of samples. While one may analyze the measurements arising from different technologies individually, additional and potentially important insights can be gained from the joint (integrated) analysis of the data sets. Joint analysis, also called multi-view or multi-modal analysis, has received considerable attention in the literature, see (Lahat et al., 2015; Meng et al., 2016; Timi et al., 2019; Pucher et al., 2019; McCabe et al., 2019) and the references therein for more details.

Here we consider a setting in which two data types, referred to as Type 1 and Type 2, with numerical features are available. We are interested in the problem of identifying pairs (A, B) , where A is a set of features of Type 1 and B is a set of features of Type 2, such that the aggregate squared correlation between features in A and B is large (see Figure 1). Moreover, we wish to carry out this identification in an unsupervised and exploratory setting that does not make use of auxiliary information about the samples or the features, and that does not rely on explicit modeling assumptions. Identifying sets of highly correlated features within a single data type has been widely studied, typically through clustering and related methods. Borrowing from the use in genomics of the term “module” to refer to a set of correlated genes, we call the feature set pairs (A, B) of interest to us *bimodules*. The term bimodule has also appeared, with somewhat different meaning, in Wu et al. (2009), Patel et al. (2010), and Pan et al. (2019).

We will refer to correlations between features of the same type as *intra-correlations*, and between features of different types as *cross-correlations*, noting that this usage differs from that in time-series analysis. Cross-correlations provide information about interactions between data types. These interactions are of interest in many applications, for example, in studying the relationships between genotype and phenotype in genomics (discussed in Section 4 below), temperature and precipitation in climate science (discussed in Section 5 below), habitation of species and their environment in ecology (see, e.g., Dray et al., 2003), in identifying brain regions associated with experimental tasks (McIntosh et al., 1996) in neuroscience (cf. references in Winkler et al. (2020) for further neuroscience applications).

Bimodules provide evidence for the coordinated activity of features from different data types. Coordination may arise, for example, from shared function, causal interactions, or more indirect functional relationships. Bimodules can assist in directing downstream analyses, generating new hypotheses, and guiding the targeted acquisition and analysis of new data. By definition, bimodules capture aggregate behavior, which may be significant when no individual pair of features has high cross-correlation, or when the cross-correlation structure between the feature groups is complex. As such, the search for bimodules can leverage low-level or complex signals among individual features to find higher order structure.

1.1 Bimodule Search Procedure and Stable Bimodules

In this paper we propose and analyze an exploratory method, BSP (bimodule search procedure), for identifying bimodules in moderate and high dimensional data sets. BSP is a testing based method that specifically targets stable bimodules. Roughly speaking, a bimodule (A, B) is *stable* if A coincides with the features of Type 1 that have significant

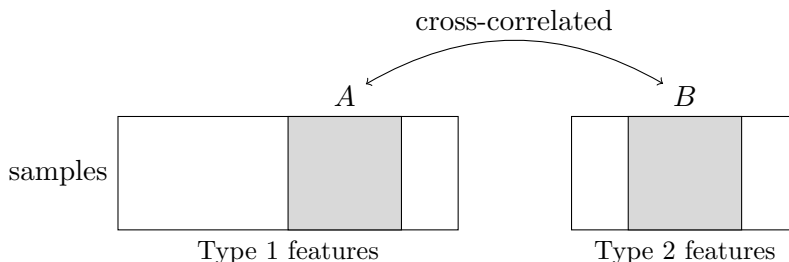


Figure 1: Illustration of multi-view data and a bimodule (A, B) (shaded). The Type 1 and Type 2 data matrices are matched by samples. The columns of A and B need not be contiguous.

aggregate squared correlation with the features in B , and B coincides with the features of Type 2 that have significant aggregate squared correlation with the features in A (a formal definition is given in Section 2).

The BSP method is not model based. Instead, it relies on a more flexible, multiple testing based approach to identify stable bimodules. The multiple testing procedures, in turn, rely on fast approximations of permutation p-values for sums of squared cross-correlations. Importantly, the permutation based p-values employed by BSP explicitly account for correlations between features of the same type, attenuating the significance of cross-correlations when intra-correlations are high. Derivation and discussion of the p-values can be found in Section 2.2.

The general definition of a bimodule raises two issues that need to be addressed in practice. The first issue is overlap: a small change in the feature sets comprising a bimodule will often yield another bimodule. As such, distinct bimodules can exhibit substantial overlap. In many applications, e.g., the study of gene regulatory networks, overlap of interacting feature sets is the norm, and the ability to capture this overlap is critical for successful exploratory analysis. Nevertheless, extreme overlap can impede interpretation and downstream analyses. We deal with overlap in two ways. First, our focus on stable bimodules eliminates most small perturbations from consideration. Second, in cases where we find two or more bimodules with large overlap, we employ a simple post-processing step to identify a representative bimodule from the overlapping group (see Section 2.5).

The second issue is containment: one or more bimodules may be contained in a larger bimodule. In practice, we wish to identify minimal bimodules, those that do not properly contain another bimodule, as such bimodules are more likely to reveal interpretable interactions between features. In practice, checking minimality of a stable bimodule can be difficult, and we rely instead on a notion of robust connectivity that leverages the connection between bimodules and the cross-correlation network arising from bi-view data. A robust bimodule cannot be partitioned into two groups without removing one or more high weight connections between the groups (see Section 2.4 for more details).

1.2 Expression Quantitative Trait Loci Analysis

Much of the existing work on bimodules is focused on the integrated analysis of genomic data. To motivate and provide context for BSP we briefly discuss the problem of expression

quantitative trait loci (eQTL) analysis in genomics. An extended application of BSP to eQTL analysis is presented in Section 4.

Genetic variation within a population is commonly studied through single nucleotide polymorphisms, called SNPs. A SNP is a single site in the genome where there is at least moderate variation in the paired nucleotides among members of the population. The value of a SNP for an individual is the number of reference nucleotides appearing at that site, which takes the values 0, 1, or 2. After normalization and covariate correction, the value of a SNP may no longer be discrete.

eQTL analysis seeks to identify SNPs that affect the expression of one or more genes. A SNP-gene pair for which the expression of the gene is correlated with the value of the SNP is referred to as an eQTL. Identification of eQTLs is an important first step in the study of genomic pathways and networks that underlie disease and development in human and other populations (see Nica and Dermitzakis, 2013; Albert and Kruglyak, 2015).

In modern eQTL studies it is common to have measurements of 10-20 thousand genes and 2-5 million SNPs on hundreds (or in some cases thousands) of samples. Identification of putative eQTLs or genomic “hot spots” is carried out by evaluating the correlation of numerous SNP-gene pairs, and identifying those meeting an appropriate multiple testing based threshold. In studies with larger sample sizes it may be feasible to carry out *trans*-eQTL analyses, which consider all SNP-gene pairs regardless of genomic location. However, it is more common to carry out *cis*-eQTL analyses, in which one restricts attention to SNP-gene pairs for which the SNP is within some fixed genomic distance (often 1 million base pairs) of the gene’s transcription start site, and in particular, on the same chromosome (c.f. Westra and Franke, 2014; GTEx Consortium, 2017). We use the prefixes *cis*- and *trans*- to refer to the type of eQTL analysis, while using adjectives *local* and *distal* to denote the proximity of the discovered SNP-gene pairs. In particular, *cis*-eQTL analyses seek to discover local eQTLs, while *trans*-eQTL analyses seek to discover *both* local and distal eQTLs.

As a result of multiple testing correction needed to address the large number of SNP-gene pairs under study, both *trans*- and *cis*-eQTL analyses can suffer from low power. Several methods have been proposed to improve the power of standard eQTL analysis, including penalized regression schemes that try to account for intra-gene or intra-SNP interactions (Tian et al., 2014, and references therein) and methods that consider gene modules as high-level phenotypes to reduce the burden of multiple-testing (Kolberg et al., 2020). As an alternative, one may shift attention from individual SNP-gene pairs to SNP-gene bimodules, that is, to sets of SNPs and genes with large cross-correlation. As genes often act in concert with one another, bimodule discovery methods can gain statistical power from group-wise interactions, by borrowing strength across individual SNP-gene pairs. Further, it is known that activity in a cell may be the result of a regulatory network of genes rather than individual genes (Chakravarti and Turner, 2016). Hence bimodules may represent a group of SNPs that disrupt the functioning of gene regulatory networks and contribute to diseases (Platig et al., 2016).

1.3 Related Work

Cross correlations in bi-view data can be represented as a bipartite network whose vertices correspond to features Type1 and Type 2: there is an edge between features of different types with weight equal to their correlation, but there are no edges between features of the same type.

The CONDOR (Platig et al., 2016) procedure identifies bimodules by applying a community detection method to an unweighted bipartite graph obtained by thresholding the weights of this cross-correlation network. One could, in principle, extend this approach by leveraging other community detected methods (Beckett, 2016; Barber, 2007; Liu and Murata, 2010; Costa and Hansen, 2014; Pesantez-Cabrera and Kalyanaraman, 2016) for weighted and unweighted bipartite networks. In another network based approach taken in Huang et al. (2009), an algorithm to enumerate bipartite cliques is used to enhance eQTL discovery.

We note that the cross-correlation network is *not* a sufficient statistic for BSP. In particular, the tests on which BSP is based account for the intra-correlations between features of the same type, which are not represented in the cross correlation network.

In seeking to uncover relationships between two data types, a number of methods identify sets of latent features that best explain the joint covariation between the two data types, often by optimizing an objective over the space spanned by the data features (see the survey Sankaran and Holmes, 2019). Sparse canonical correlation analysis (sCCA) (Waaaijenborg et al., 2008; Witten et al., 2009; Parkhomenko et al., 2009) finds pairs of sparse linear combinations of features from the two data types that are maximally correlated. One may regard each such canonical covariate pair as a bimodule consisting of the features appearing in the linear combination.

In the context of eQTL analysis, methods based on Gaussian graphical models Cheng et al. (2012, 2015, 2016) and penalized multi-task regression Chen et al. (2012) have also been used to find bimodules. In the former work, the authors fit a sparse graphical model with a hidden variables that model interactions between groups of genes and groups of SNPs. In Chen et al. (2012), the gene and SNP networks derived from the respective intra-correlations matrices are used in a penalized regression setup to find a network-to-network mapping in the same spirit as bimodules.

One may also search for bimodules by applying a standard clustering method such as k-means to a joint data matrix containing standardized features from the two data types, and treating any cluster with features from both data types as a bimodule. While appropriate as a “first look”, this approach requires specifying the number of clusters, imposes the constraint that every feature be part of one, and only one, bimodule, and, most importantly, does not distinguish between cross- and intra-correlations.

1.4 Overview of the Paper

The next section presents the testing-based definition of stable bimodules based on p-values derived from a permutation null distribution, and the Bimodule Search Procedure. Section 3 is devoted to a simulation study that makes use of a complex model to capture some of the features observed in real bi-view data. Here we compare the performance of BSP with CONDOR and sCCA. Section 4 describes and evaluates the results of BSP and CONDOR

applied to an eQTL dataset from the GTEx consortium. In particular, we examine the bimodules produced by BSP using a variety of descriptive and biological metrics, including comparisons with, and potential extensions of, standard eQTL analysis. In Section 5, we present the results of BSP applied to inter-annual temperature and precipitation measurements in North America.

2. Stable Bimodules and the Bimodule Search Procedure

2.1 Introducing notation and the stability criteria

Let \mathbb{X} be an $n \times p$ matrix containing data of Type 1, and let \mathbb{Y} be an $n \times q$ matrix containing data of Type 2. The columns of \mathbb{X} and \mathbb{Y} correspond to features of Type 1 and Type 2, respectively. The i th row of \mathbb{X} (\mathbb{Y}) contains measurements of Type 1 (Type 2) on the i th sample. Features of Type 1 will be indexed by $S = \{s_1, s_2, \dots, s_p\}$, features of Type 2 by $T = \{t_1, t_2, \dots, t_q\}$. Let \mathbb{X}_s be the column of \mathbb{X} corresponding to feature s , and let \mathbb{Y}_t be the column of \mathbb{Y} corresponding to feature t . For $s \in S$ and $t \in T$ let $r(s, t)$ be the sample correlation between \mathbb{X}_s and \mathbb{Y}_t . For $A \subseteq S$ and $B \subseteq T$, define the aggregate squared correlation between A and B by

$$r^2(A, B) \doteq \sum_{s \in A, t \in B} r^2(s, t). \quad (1)$$

For singleton sets we will omit brackets, writing $r^2(s, B)$ and $r^2(A, t)$.

Recall that our goal is to identify pairs (A, B) with $A \subseteq S$ and $B \subseteq T$ such that the aggregate cross-correlation between features in A and B is large. To this end, one may seek to maximize a score based on $r^2(A, B)$ subject to a penalty on the cardinalities of A and B , or to formulate and fit a model for \mathbb{X} and \mathbb{Y} that incorporates bimodule-type structures. While both these approaches have merit, finding computationally tractable solutions often requires detailed assumptions about the distribution of the data matrices, which can be difficult to verify in practice, as well as the introduction of free parameters that require downstream fitting.

Here we take a different, potentially more flexible, approach that is built on sequential testing of the sum-of-squared correlation statistics $r^2(s, B)$ and $r^2(A, t)$. In particular seek bimodules (A, B) that are stable in the sense that A is exactly the set of features in $s \in S$ for which $r^2(s, B)$ is significant at some given false discovery rate, and B is exactly the set of features in $t \in T$ for which $r^2(A, t)$ is significant at the same false discovery rate. If it is non-empty, a stable bimodule has large aggregate cross-correlations, which are significant in a singleton-to-set sense. Moreover, the definition can be viewed as a fixed point condition, which motivates the iterative BSP method to find stable bimodules described below.

The next subsection describes the permutation based p-values that we use to assess the significance of the statistics $r^2(s, B)$ and $r^2(A, t)$. Stable bimodules are defined in Section 2.3. The bimodule search procedure is described in Section 2.4.

2.2 Permutation Null Distribution and P-values

In what follows we assume that the data $[\mathbb{X}, \mathbb{Y}]$ is fixed.

Definition 1 Let $P_1, P_2 \in \{0, 1\}^{n \times n}$ be chosen independently and uniformly from the set of all $n \times n$ permutation matrices. The permutation null distribution of $[\mathbb{X}, \mathbb{Y}]$ is the distribution of the data matrix $[\tilde{\mathbb{X}}, \tilde{\mathbb{Y}}] \doteq [P_1 \mathbb{X}, P_2 \mathbb{Y}]$.

The permutation null distribution is obtained by randomly reordering the rows of \mathbb{X} and, independently, the rows of \mathbb{Y} . Let \mathbb{P}_π and \mathbb{E}_π denote probability and expectation, respectively, under the permutation null. For $s \in S$ and $t \in T$ let $R(s, t)$ be the (random) sample-correlation of $\tilde{\mathbb{X}}_s$ and $\tilde{\mathbb{Y}}_t$ under the permutation null. Permutation preserves the sample correlation between the features in S , and between the features in T , but nullifies cross-correlations between S and T . Indeed, as shown in Zhou et al. (2013), $\mathbb{E}_\pi[R(s, t)] = 0$ for each $s \in S$ and $t \in T$.

Definition 2 For $A \subseteq S$ and $B \subseteq T$ define the permutation p-value

$$p(A, B) \doteq \mathbb{P}_\pi(R^2(A, B) \geq r^2(A, B)) \quad (2)$$

where $R^2(A, B) \doteq \sum_{s \in A, t \in B} R^2(s, t)$ and the observed sum of squares $r^2(A, B)$ is fixed.

Small values of $p(A, B)$ provide evidence against the null hypothesis that the aggregate cross-correlation between features in A and B is zero. As the permutation distribution preserves the correlations between features of the same type, the p-value $p(A, B)$ accounts for the effects of these correlations when assessing the significance of $r^2(A, B)$.

There is no simple closed form expression for the p-values $p(A, B)$, and direct approximation via permutation is computationally prohibitive in the context of the BSP procedure (Section 2.4); indeed, in each iteration, BSP requires an estimate of $|S| + |T|$ p-values of the form $\{p(s, B)\}_{s \in S}$ and $\{p(A, t)\}_{t \in T}$. Here we adapt ideas from Zhou et al. (2013) and Zhou et al. (2019) to approximate the permutation p-values $p(A, t)$ (or $p(s, B)$) using the tails of a location-shifted Gamma distribution that has the same first three moments as the sampling distribution of $R^2(A, t)$ under the permutation null. As shown in (Zhou et al., 2013), while the first permutation moment satisfies $\mathbb{E}_\pi R^2(A, t) = \frac{|A|}{(n-1)}$, the next two moments can be computed exactly in $O(n^3)$ steps. However, to further speed computation, we use instead the eigenvalue conditional moment formulas for the second and third moments of $R^2(A, t)$ (see Zhou et al., 2019), which depend only on the eigenvalues of the intra-correlation matrix of the features in A and not on t . The analytical formula for the eigenvalue conditional moments of $R^2(A, t)$ is derived in Zhou et al. (2019) by conditioning on the observed eigenvalues of the intra-correlation matrix for features $\tilde{\mathbb{X}}_A \doteq \{\tilde{\mathbb{X}}_s\}_{s \in A}$ under the assumption that the rows of $\tilde{\mathbb{X}}$ are i.i.d. multivariate normal vectors; however in place of the normality assumption, it is sufficient to have the weaker assumption of distributional invariance of $\tilde{\mathbb{X}}_A$ under left-multiplication by $n \times n$ orthogonal matrices. In practice, the additional assumptions used in the moment approximation do not appear to limit the applicability of BSP. Accuracy of the p-value approximations is briefly discussed in Appendix A.5.

2.3 Stable Bimodules

In order to define stable bimodules, we use the multiple testing procedure of Benjamini and Yekutieli (2001) (B-Y) to assess the significance of the observed values of $r^2(s, B)$ and

$r^2(A, t)$ under the permutation null distribution. Let $p = p_1, \dots, p_m \in [0, 1]$ be the p-values associated with a family of m hypothesis tests, with order statistics $p_{(1)} \leq p_{(2)} \dots \leq p_{(m)}$. Given a target false discovery rate $\alpha \in (0, 1)$, the B-Y procedure rejects the hypotheses associated with the p-values $p_{(1)}, \dots, p_{(k)}$ where

$$p_{(k)} = \max \left\{ p_{(j)} : \frac{m p_{(j)}}{j} \leq \frac{\alpha}{\sum_{i=1}^m i^{-1}} \right\} \doteq \tau_\alpha(p) \quad (3)$$

As shown in Benjamini and Yekutieli (2001), regardless of the joint distribution of the p-values in p , the expected value of the false discovery rate among the rejected hypotheses is at most α . The value $\tau_\alpha(p)$ acts as an adaptive significance threshold: given p , we reject the hypothesis associated with p_j if and only if $p_j \leq \tau_\alpha(p)$.

Definition 3 (*Stable Bimodule*) Let $[\mathbb{X}, \mathbb{Y}]$ and $\alpha \in (0, 1)$ be given. A pair (A, B) of non-empty sets $A \subseteq S$ and $B \subseteq T$ is a stable bimodule at level α if

1. $A = \{s \in S : p(s, B) \leq \tau_\alpha(p_B)\}$ and
2. $B = \{t \in T : p(A, t) \leq \tau_\alpha(p_A)\}$

where $p_B = \{p(s, B)\}_{s \in S}$ and $p_A = \{p(A, t)\}_{t \in T}$.

Stable bimodules enable the aggregation of small effects across feature pairs. The condition $p(s, B) \leq \tau_\alpha(p_B)$ can be written equivalently as $r^2(s, B) \geq \hat{\gamma}(s, B)$ where the correlation threshold $\hat{\gamma}(s, B)$ depends on s , B , and p_B . The latter condition may be satisfied even if the feature s is not significantly correlated with any *individual* feature in B . Similar remarks apply to $p(A, t)$.

While stable bimodules depend critically on the observed cross-correlations $r(s, t)$, they *cannot* be recovered from the sample cross-correlation matrix or the associated cross-correlation network alone. This is because the thresholds $\hat{\gamma}(s, B)$ and $\hat{\gamma}(A, t)$ also depend on other aspects of the data, most critically the intra-correlations of features in A and B , through the p-values p_A and p_B .

A likely side-effect of any directed search for bimodules (A, B) , stable or otherwise, is that the sample intra-correlations of the features in A and B will be large, often significantly larger than the intra-correlations of a randomly selected set of features with the same cardinality. Failure to account for inflated intra-correlations will lead to underestimates of the standard error of most test statistics, including the sum of squared correlations used here, which will in turn lead to anti-conservative (optimistic) assessments of significance, and oversized feature sets. As noted above, the permutation distribution leaves intra-correlations unchanged, while ensuring that cross-correlations are equal to zero. In this way the permutation p-values $p(s, B)$ and $p(A, t)$ directly account for the effects of intra-correlations among features in B and A , respectively.

2.4 The Bimodule Search Procedure (BSP)

Let 2^S and 2^T denote the collection of all subsets of S and T , respectively. Definition 3 says that stable bimodules are exactly the non-empty fixed points of the (data dependent) map $\hat{\Gamma} : 2^S \times 2^T \rightarrow 2^S \times 2^T$ defined by $\hat{\Gamma}(A, B) = (A', B')$ where $B' = \{t \in T : p(A, t) \leq \tau_\alpha(p_A)\}$

and $A' = \{s \in S : p(s, B') \leq \tau_\alpha(p_{B'})\}$. A natural procedure to find stable bimodules is to repeatedly apply the map $\hat{\Gamma}$ starting from an initial pair (A_0, B_0) until a fixed point is reached or the sets eventually cycle. The result is the Bimodule Search Procedure (BSP). We assume in what follows that $|S| \leq |T|$.

Input: Data matrices \mathbb{X} and \mathbb{Y} and parameter $\alpha \in (0, 1)$.

Output: A stable bimodule (A, B) at level α , if found.

```

1 initialize:  $A' = \{s\} \subseteq S$  and  $A = B = B' = \emptyset$ ;
2 while  $(A', B') \neq (A, B)$  do
3    $(A, B) \leftarrow (A', B')$ ;
4   Compute  $p(A, t)$  for each  $t \in T$  and let  $p_T \leftarrow (p(A, t))_{t \in T}$ ;
5    $B' \leftarrow \{t \in T : p(A, t) \leq \tau_\alpha(p_T)\}$ ; // Indices rejected by B-Y
6   Compute  $p(s, B')$  for each  $s \in S$  and let  $p_S \leftarrow (p(s, B'))_{s \in S}$ ;
7    $A' \leftarrow \{s \in S : p(s, B') \leq \tau_\alpha(p_S)\}$ ; // Indices rejected by B-Y
8 end
9 if  $|A||B| > 0$  and  $(A, B) = (A', B')$  then
10 | return  $(A, B)$ ;
11 end

```

Algorithm 1: Bimodule Search Procedure (BSP)

Pseudo-code for the Bimodule Search Procedure is given in Algorithm 1. As the procedure operates in a deterministic manner, and the number of feature set pairs is finite, the iterative search procedure is guaranteed to terminate at a fixed point or enter a limiting cycle. A fixed point can be empty ($A = B = \emptyset$) or non-empty ($A, B \neq \emptyset$). Non-empty fixed points are stable bimodules at level α . To limit computation time and address the possibility of cycles, the BSP is terminated at 20 iterations. In our simulations and real-data analyses (described below) the 20 iteration limit was rarely reached. In practice cycles are rare, and most initial conditions lead to empty fixed points. For instance, in the eQTL application (Section 4), BSP runs were started from $\sim 304\text{K}$ initial conditions, the majority ($\sim 277\text{K}$) of which found an empty fixed point within the first few iterations. Of the remaining 27K searches, the great majority identified a non-empty fixed point within 20 steps. Only 20 searches cycled and did not terminate in a fixed point.

In practice, BSP is run repeatedly, initializing with every singleton set $\{s\}$ for $s \in S$, resulting in a list of non-empty bimodules, which may contain overlapping bimodules as well as repeats. In order to limit the number potentially spurious bimodules, and to limit the number of bimodules containing a single pair, we remove from the list any bimodule (A, B) for which $p(A, B)$ exceeds the Bonferroni threshold $\alpha/|A||B|$ for singleton bimodules. Denote the resulting list by $\mathcal{B} = (A_1, B_1), \dots, (A_N, B_N)$. Post-processing of \mathcal{B} to control overlap and network-based assessment of minimality are discussed in Section 2.5 and Section 2.6 below.

The false discovery rate $\alpha \in (0, 1)$ used in the B-Y multiple testing procedures is the only free parameter of the BSP. While α controls the false discovery rate of features s or t at each step of the search procedure, it does not guarantee control of the false discovery rate of pairs (s, t) within stable bimodules. In general, BSP will find fewer and smaller bimodules when α is small, and will find more numerous and larger bimodules when α is

large. In practice, we employ a permutation based procedure to select α from a fixed grid of values based on the notion of *edge-error* discussed in Section 3. Details can be found in Appendix A.3.

Iterative testing procedures have been applied in single data-type settings for community detection in unweighted Wilson et al. (2014) and weighted Palowitch et al. (2016) networks, differential correlation mining Bodwin et al. (2018), and association mining for binary data Mosso et al. (2017). In these papers a stable set of significant nodes or features is identified through the iterative application of multiple testing. However, the hypotheses of interest and the associated test statistics all differ substantially from the setting here. Moreover, the p-values in these papers were derived from asymptotic normal and binomial approximations, rather than the more complicated permutation moment fitting used here.

2.5 Post-processing of Bimodules to Address Overlap

Recall that $\mathcal{B} = (A_1, B_1), \dots, (A_N, B_N)$ is the list of stable bimodules found by BSP after initial filtering to remove bimodules such that $p(A, B)$ exceeds the Bonferroni threshold $\alpha/|A||B|$ for singletons. In general, the same bimodule may appear multiple times in \mathcal{B} , and bimodules in \mathcal{B} may overlap. To address this, we first assess the effective cardinality N_e of \mathcal{B} , then identify N_e groups of related bimodules in \mathcal{B} , and finally select a representative bimodule from each group. Details are given below.

Let $C_j = A_j \times B_j$ be the set of (s, t) pairs in the j th bimodule of \mathcal{B} . Following Shabalin et al. (2009) we define the *effective number* of bimodules in \mathcal{B} as

$$N_e \doteq \sum_{C \in \mathcal{B}} \left\{ \frac{1}{|C|} \sum_{(s,t) \in C} \frac{1}{\sum_{C' \in \mathcal{B}} \mathbb{I}((s,t) \in C')} \right\} \quad (4)$$

Note that $0 \leq N_e \leq N$, and if \mathcal{B} contains r distinct bimodules with disjoint index sets (and arbitrary multiplicity) in \mathcal{B} then $N_e = r$. With N_e in hand, we apply agglomerative hierarchical clustering to the bimodules in \mathcal{B} using average linkage and a dissimilarity measure equal to the Jaccard distance between the index sets,

$$d_J(C, C') = 1 - \frac{|C_1 \cap C_2|}{|C_1 \cup C_2|}.$$

We then prune the resulting dendrogram by selecting the horizontal cut that yields closest to N_e clusters. Finally, from each of the resulting clusters $\mathcal{C} \subseteq \mathcal{B}$ we select a representative bimodule $C \in \mathcal{C}$ maximizing the centrality score

$$\eta(C : \mathcal{C}) = \sum_{(s,t) \in C} \sum_{C' \in \mathcal{C}} \mathbb{I}((s,t) \in C'). \quad (5)$$

The centrality score $\eta(C : \mathcal{C})$ favors bimodules C whose elements are contained in many of the other bimodules C' falling in the cluster \mathcal{C} .

2.6 Network-Based Assessment of Minimality

A stable bimodule is minimal if it does not properly contain a stable bimodule. Minimal bimodules represent indecomposable structures, which may enhance their interpretability

in exploratory tasks. Initializing BSP with singletons encourages the discovery of minimal bimodules, but in general, the bimodules output by BSP are not guaranteed to be minimal. As verifying minimality in practice can be computationally prohibitive, we adopt an alternative, network based approach to assess the decomposability of stable bimodules found by BSP.

We begin with the sample cross-correlation network G_s , which is a weighted bipartite network with vertex set $S \cup T$ and edge set $E = S \times T$. Each edge (s, t) has weight $w(s, t)$ equal to the observed sample correlation $r(s, t)$ between features \mathbb{X}_s and \mathbb{Y}_t . Note that G_s has no edges between features of the same type. For each $\tau \geq 0$, let $G_s(\tau)$ be the subgraph of G_s obtained by removing edges (s, t) with absolute weight $|w(s, t)| \leq \tau$; let $E(\tau)$ denote the resulting set of edges. A feature pair (A, B) is connected in $G_s(\tau)$ if there is a path (a sequence of adjacent edges in $E(\tau)$) connecting every distinct pair of indices $u, v \in A \cup B$.

Definition 4 *The connectivity threshold $\tau^*(A, B)$ of a feature set pair (A, B) is the largest $\tau \geq 0$ such that (A, B) is connected in $G_s(\tau)$. The essential edges of (A, B) are the pairs $(s, t) \in A \times B$ such that $|r(s, t)| \geq \tau^*(A, B)$.*

Consideration of the connectivity threshold and essential edges is motivated in part by asymptotic analysis, reviewed in the next section, which shows that the counterpart to a minimal stable bimodule in the large sample limit is a connected component of the population cross correlation network. The threshold $\tau^*(A, B)$ measures the strength of the weakest link needed to maintain connectivity of the features $A \cup B$ in G_s . In other words, the feature set $A \cup B$ cannot be partitioned into two non-empty groups without removing an edge of magnitude at least $\tau^*(A, B)$. In this way $\tau^*(A, B)$ quantifies the ease with which the bimodule (A, B) can be decomposed into a disjoint union of smaller bimodules. In practice, the bimodules found by BSP have relatively high connectivity thresholds (e.g. see Section 4.2.3), indicating that these bimodules are robustly connected.

One may regard $E(\tau) \cap (A \times B)$ as an estimate of the feature pairs $(s, t) \in A \times B$ that are truly correlated at the population level, with larger values of τ leading to more conservative estimates. The value $\tau = \tau^*(A, B)$ is the most conservative threshold subject to the constraint that $A \cup B$ is connected in $G_s(\tau)$, and the essential edges are those of the resulting graph.

2.7 Overview of Asymptotic Theory for BSP

We briefly discuss some theoretical results from ongoing work (Dewaskar and Nobel, 2022), which can be used to study the behavior of BSP in the large n and small p (and q) asymptotic regime. These results are proved under the assumption that the rows of data matrix $D_n = [\mathbb{X}, \mathbb{Y}]$ are i.i.d. copies of a $(p + q)$ -dimensional jointly Gaussian vector $[\mathbf{X}, \mathbf{Y}] \doteq [X_{s_1}, \dots, X_{s_p}, Y_{t_1}, \dots, Y_{t_q}]$. An important role will be played by the *population cross-correlation network* G_p associated with the distribution of $[\mathbf{X}, \mathbf{Y}]$; G_p is the unweighted bipartite network consisting of two types of vertices S and T , and edges formed by pairs $(s, t) \in S \times T$ such that the variables X_s and Y_t have a non-zero population cross-correlation.

Given the random data D_n , let $\Gamma_n^\alpha : 2^S \times 2^T \rightarrow 2^S \times 2^T$ denote the one-step update map used in BSP (more precisely, this is the map $\hat{\Gamma}$ defined at the beginning of Section 2.4) applied to the data D_n with false discovery parameter α . A key step in obtaining

asymptotic results for BSP is to identify a deterministic map $\Gamma : 2^S \times 2^T \rightarrow 2^S \times 2^T$ that is the limit of the random maps Γ_n^α , for a suitable choice of $\alpha = \alpha_n$, as $n \rightarrow \infty$. If this is established, the fixed points of Γ serve as natural population level targets for the bimodule search procedure.

In the asymptotic regime where n grows faster than $\max(p^2, q^2)$, and α_n is chosen suitably small, the limiting update map $\Gamma : 2^S \times 2^T \mapsto 2^S \times 2^T$ can be identified in terms of neighbors in the population cross-correlation network G_p . More precisely, $\Gamma(A, B) = (A', B')$, where B' denotes the set of neighbors of A , and A' denotes the set of neighbors of B' in the graph G_p . Further examination shows that the minimal fixed points of Γ , called *population bimodules*, are precisely the set of connected components of G_p with two or more vertices; moreover, these minimal fixed points can be reached by iterating the map Γ starting from suitable singleton initial sets of the form $A_0 = \{s\} \subseteq S$ and an arbitrary $B_0 \subseteq T$. Connecting all of this together, one can show that BSP iterations starting from singleton sets of features will, in the limit as $n \rightarrow \infty$, find stable bimodules that are connected components of G_p with two or more vertices. Note, however, that under the high-dimensional asymptotic regime where $\min(p, q)$ grows faster than n , BSP could have potentially different and more nuanced behavior. This is an important topic for further investigation.

3. Simulation Study

To assess the effectiveness of BSP, we simulated a dataset on $n = 200$ samples with $p = 100,000$ and $q = 20,000$ features of Types 1 and 2, respectively. The data was generated from a model with $K = 500$ disjoint *target* bimodules of various sizes, (intra- and cross-) correlation strengths, and network structures at the population level. Simulation studies incorporating fewer than ten embedded bimodules have been conducted for methods based on sCCA (Waaaijenborg et al., 2008; Parkhomenko et al., 2009; Witten et al., 2009) and graphical models (Cheng et al., 2016, 2015). Motivated by the eQTL analysis application in Section 4, we considered a more sophisticated simulation model that incorporates a diverse collection of target bimodules and related network structures. To make the recovery of these bimodules more challenging, edges were added at random between target bimodules so that the population cross-correlation network has a so-called giant connected component. Large connected components have been observed in empirical eQTL-networks (Platig et al., 2016; Fagny et al., 2017). Details concerning the simulation model can be found in Appendix B.1.

We ran BSP, CONDOR, and sCCA on the simulated datasets. The parameter $\alpha = 0.01$ for BSP was chosen to control an estimate of the edge-error (defined below) derived from partially permuted instances of the observed data. See Appendix B.2 for how the free parameters for other procedures were selected. We compared the results from each method to the ground truth to assess (a) the recovery of target bimodules by each method, and (b) the presence of spurious associations within the bimodules detected by these methods. To evaluate (a) we calculated the largest Jaccard similarity between each target bimodule and a detected bimodule. For (b) we evaluated the *edge-error* of each detected bimodule, which is defined as the fraction of essential-edges of the detected bimodule that are not contained in a target bimodule or the set of confounding edges.

Figure 2 (left) shows the recovery of target bimodules by BSP. The performance of BSP was influenced primarily by the cross-correlation strength $\sqrt{\frac{r^2(A,B)}{|A||B|}}$ of the target bimodule, though the intra-correlation strength (measured by the parameter ρ from Equation 8 in Appendix B.1) also had an effect. Most target bimodules with cross-correlation strength above 0.4 were completely recovered, while those with strength below 0.2 were not recovered. For strengths between 0.2 to 0.4, there was a variation in recovery, with smaller Jaccard similarity for bimodules having larger intra-correlation strength. The effect of intra-correlation strength on recovery was expected as BSP accounts for the intra-correlations among features of the same type. While not guaranteed, BSP does a good job of controlling false discoveries: the average edge-error for BSP bimodules was 0.03, and 90% of the BSP-bimodules had edge-error under 0.05.

The results from CONDOR and sCCA on the simulation study are described in detail in Appendix B.2.1, but we highlight some key points here. The recovery of a target bimodules by CONDOR was rather insensitive to intra-correlation strength, so we only considered the effect of cross-correlations. As CONDOR bimodules often contained multiple target bimodules, we used an inclusion based notion of recovery, denoted as *recall*, rather than Jaccard similarity, which emphasizes equality of bimodules. (The two recovery metrics *recall* and *Jaccard* are defined in Appendix B.2.1.) With this metric, the average recovery curves for CONDOR and BSP, as a function of the cross-correlation strength, were comparable. CONDOR bimodules had a larger average edge-error of 0.08, which could have arisen because the method did not account for intra-correlations.

Concerning sCCA, the detected bimodules were very large and had a high average edge-error of 0.89 when we used the default parameter choice. We also ran the procedure with a range of parameters that yielded smaller bimodules, but the recovery and edge-error of the procedure continued to lag behind those of BSP and CONDOR (see Appendix B.4.2).

We also studied the performance of BSP and CONDOR on a simulation study with larger sample size $n = 600$. As expected, both methods were able to recover bimodules with lower cross-correlation strengths than earlier, in terms of *recall*. However, both BSP and CONDOR had lower recovery than in the $n = 200$ simulation (Appendix B.3), in terms of Jaccard similarity. We briefly discuss this behavior in Section 6.

4. Application of BSP to eQTL Analysis

Here we describe the application of bimodules to the problem of expression quantitative trait loci (eQTL) analysis discussed in Section 1. The NIH funded GTEx Project has collected and created a large eQTL database containing genotype and expression data from postmortem tissues of human donors. We applied BSP, CONDOR, and standard eQTL-analysis to $p = 556,304$ SNPs and $q = 26,054$ thyroid expression measurements from $n = 574$ individuals. A detailed account of data acquisition, preprocessing, and covariate correction can be found in Appendix C.1.

4.1 Running BSP and other methods

We applied BSP to the thyroid eQTL data with false discovery parameter $\alpha = 0.03$, selected using a permutation-based procedure to keep the edge-error estimates under 0.05 (details

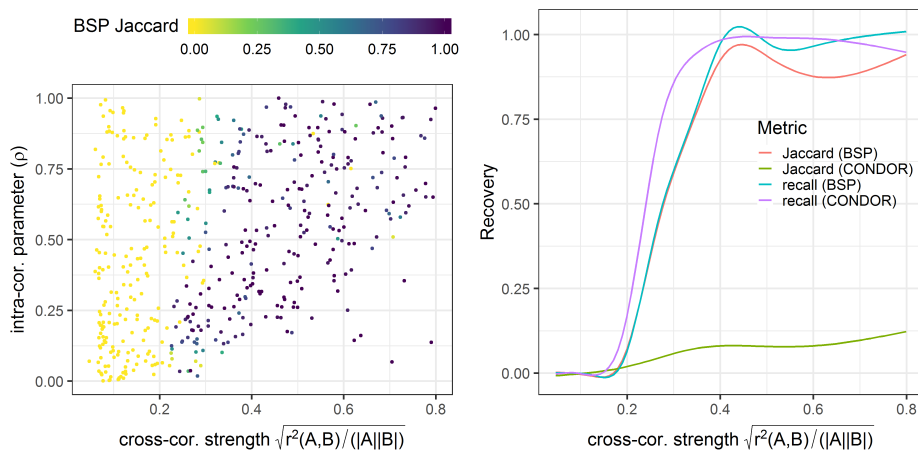


Figure 2: Recovery of target bimodules under the equality based metric *Jaccard* and the inclusion based metric *recall* (Appendix B.2.1). Left: dependence of cross-correlation strength and intra-correlation parameter of target bimodules on BSP Jaccard. Right: the averaged recovery curves (recall and Jaccard) for target bimodules under CONDOR and BSP as a function of their cross-correlation strength.

in Appendix C.4). The search produced 3744 unique bimodules; the effective number of bimodules was 3304. We applied the filtering procedure described in Section 2.5 to select from a subfamily of 3304 bimodules that were substantially disjoint. More details concerning implementation of BSP, including initialization, convergence, and running times can be found in Appendix C.2.

We also performed standard *cis*- and *trans*-eQTL analysis on the thyroid eQTL data using Matrix-eQTL (Shabalin, 2012), and applied CONDOR (Platig et al., 2016) and sCCA (Witten et al., 2009) to produce bimodules. Details about the pipeline and parameter choices can be found in Appendix C.3. CONDOR produced six bimodules in total; sCCA was tasked with identifying 50 bimodules. Figure 3 shows the sizes of the bimodules identified by the various methods. All bimodules identified by sCCA were very large, making them difficult to analyze and interpret. The identified bimodules also exhibited moderate overlap: the effective number was 25. As such, we excluded the sCCA bimodules from subsequent comparisons. However, analysis of sCCA on the simulated data (Appendix B.4.2) suggests that the method may be able to recover smaller bimodules with a more tailored choice of its parameters.

4.2 Quantitative Validation

In this subsection, we apply several objective measures to validate and understand the bimodules found by BSP and CONDOR.

4.2.1 PERMUTED DATA

In order to assess the propensity of each method to detect spurious bimodules, we applied BSP and CONDOR to five data sets obtained by jointly permuting the sample labels for

the expression measurements and most covariates (all except the five genotype PCs), while keeping the labels for genotype measurements and genotype covariates unchanged. Each data set obtained in this way is a realization of the permutation null defined in Definition 1. BSP found very few (5-12) bimodules in the permuted datasets compared to the real data (3344). CONDOR found no bimodules in any of the permuted datasets.

4.2.2 BIMODULE SIZES

Most (89%) of the bimodules found by BSP have fewer than 4 genes and 50 SNPs, but BSP also identified moderately sized bimodules having 10-100 genes and 30-1000 SNPs (see Figure 3). The bimodules found by CONDOR were moderately sized, with 10-100 genes and several hundred SNPs, except for one smaller bimodule with 5 genes and 43 SNPs. On the permuted data, most bimodules found by BSP have fewer than 2 genes and 2 SNPs. As a one dimensional measure of size, we define the *geometric size* of a bimodule (A, B) to be $\sqrt{|A||B|}$, the square root of the number of gene-SNP pairs in the bimodule.

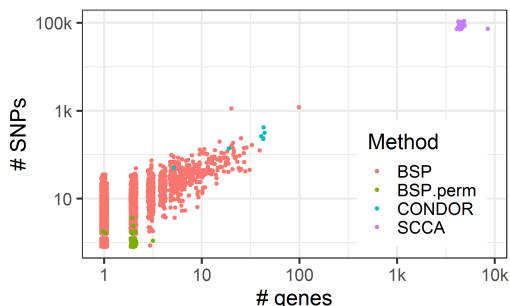


Figure 3: The sizes of bimodules detected by BSP, CONDOR and sCCA, and sizes of bimodules detected by BSP under the 5 permuted datasets.

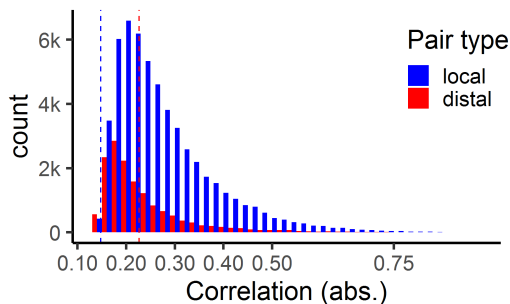


Figure 4: Correlations corresponding to SNP-gene pairs that appear as essential-edges (Section 2.6) in one or more BSP bimodules with geometric size above 10. Local pairs to the left of the blue line (*cis*-analysis threshold) and distal pairs to the left red line (*trans*-analysis threshold) show importance at the network level but were not discovered by standard eQTL analysis.

4.2.3 CONNECTIVITY THRESHOLD AND NETWORK SPARSITY

Stable bimodules capture aggregate association between groups of SNPs and genes. In some cases one may wish to identify individual SNP-gene associations of interest within discovered bimodules. A natural starting point for this is the network of essential edges of the bimodule, defined in Section 2.6. To better understand the structure of this network of essential edges, we calculate the *tree-multiplicity*

$$\text{TreeMul}(A, B) \doteq \frac{|\text{essential-edges}(A, B)|}{|A| + |B| - 1}, \tag{6}$$

which measures the number of essential edges relative to the number of edges in a tree on the same vertex set. $\text{TreeMul}(A, B)$ is never less than 1, and takes the value 1 exactly when the essential edges form a tree.

For bimodules found by BSP, the connectivity thresholds ranged from 0.14 to 0.59 and tree-multiplicities ranged from 1 to 10 (see Figure 10 in Appendix C.6). Smaller bimodules had larger connectivity thresholds and smaller tree multiplicities. As such, these bimodules had tree-like essential edge networks comprised of strong (and typically local, see Section 4.3.2) SNP-gene associations. Larger bimodules had lower connectivity thresholds and larger tree multiplicities. As such, these bimodules had more redundant essential edge networks comprised of weaker (and often distal, see Section 4.3.2) SNP-gene associations. While the essential edge networks for larger bimodules had tree-multiplicities around 10 (Figure 10, Appendix C.6), these networks were still sparsely connected compared to the complete bipartite graph on the same nodes.

4.3 Biological Validation

In order to assess the potential biological utility of bimodules found by BSP, we compared the SNP-gene pairs in bimodules to those found by standard *cis*- and *trans*-eQTL analyses. In addition, we studied the locations of the SNPs, and examined the gene sets for enrichment of known functional categories.

4.3.1 COMPARISON WITH STANDARD eQTL ANALYSIS

As described earlier, the bimodules produced by CONDOR are derived in a direct way from SNP-gene pairs identified by *cis*- and *trans*-eQTL analyses. Table 1 compares the eQTL pairs identified by standard analyses with those found in bimodules identified by BSP. Recall that *cis*-eQTL analysis considers only local SNP-gene pairs, which improves detection power by reducing multiple testing, while *trans*-eQTL analysis and BSP do not use any information about the absolute or relative genomic locations of the SNPs and genes. We find that half of the pairs identified by *cis*-eQTL analysis and most of the pairs identified by *trans*-eQTL analysis appear in at least one bimodule.

Bimodules capture sub-networks of SNP-gene associations rather than individual eQTLs, and as such individual SNP-gene pairs in a bimodule need not be eQTLs. In fact, as noted above, the detected networks underlying large bimodules are typically sparse relative to the complete network on the genes and SNPs of the bimodule. We will say that a bimodule (A, B) is connected by a set of eQTLs if the bipartite graph with vertex set $A \cup B$ and edges restricted to the set of eQTLs is connected. As shown in Table 1, a significant fraction of BSP bimodules are not connected by SNP-gene pairs obtained by *cis*-eQTL and *trans*-eQTL analysis, respectively. The discovery of such bimodules suggests that the sub-networks identified by BSP cannot be found by simple post processing of results from standard eQTL analyses. Hence the sub-networks identified by BSP may provide new insights and hypotheses for further study.

To identify potentially new eQTLs using BSP, we examine bimodule connectivity under the combined set of *cis*- and *trans*-eQTLs. All of the bimodules with one SNP or one gene are connected by the combined set of eQTLs (Appendix C.7), and therefore all edges in these singleton bimodules are discovered by standard analyses. On the other hand, 224 out of the 358 bimodules with geometric size larger than 10 were not connected by the combined set of eQTLs. In Figure 4, we plot the correlations corresponding to SNP-gene pairs that appear as essential-edges in one or more bimodules with geometric size above

Analysis type	% eQTLs found among bimodules	% bimodules connected by eQTLs
<i>trans</i> -eQTL analysis	84%	70%
<i>cis</i> -eQTL analysis	51%	88%

Table 1: Comparison of BSP and standard eQTL analysis. A gene-SNP pair is said to be found among a collection bimodules if the gene and SNP are both part of some common bimodule. On the other hand, we say that a bimodule is connected by a collection of eQTLs if under the gene-SNP pairs from the collection, the bimodule forms a connected graph.

10, along with the correlation thresholds for *cis*-eQTL (blue line) and *trans*-eQTL (red line) analyses. Around 300 local edges (i.e. the SNP is located within 1MB of the gene transcription start site) and 8.8K distal edges do not meet the correlation thresholds for *cis*- and *trans*-eQTL analysis, respectively, but show evidence of importance at the network level, and may be worthy of further study.

4.3.2 GENOMIC LOCATIONS

We studied the chromosomal location and proximity of SNPs and genes from bimodules found by BSP and CONDOR. While CONDOR uses genomic locations as part of the *cis*-eQTL analysis in its first stage, BSP does not make use of location information. Genetic control of expression is often enriched in a region local to the gene (GTEx Consortium, 2017). All CONDOR bimodules, and almost all (99.3%) BSP bimodules, have at least one local SNP-gene pair (the SNP is located within 1MB of the gene transcription start site). In 93.5% of the smaller BSP bimodules (geometric size 10 or smaller) and 54.8% of the medium to large BSP bimodules (geometric size above 10) each gene and each SNP had a local counterpart SNP or gene within the bimodule.

For each bimodule, we examined the chromosomal locations of its SNPs and genes. All SNPs and many of the genes from the six CONDOR bimodules were located on Chromosome 6; two CONDOR bimodules also had genes located on Chromosome 8 and Chromosome 9. The SNPs and genes from the BSP bimodules were distributed across all 23 chromosomes: 170 of the 2947 small bimodules spanned 2 to 5 chromosomes and 152 of the 358 medium to large bimodules spanned 2 to 11 chromosomes; the remaining bimodules were localized to a single chromosome, which varied from bimodule to bimodule.

Figure 5 illustrates the genomic locations of two bimodules found by BSP, with SNP location on the left and gene location on the right (only active chromosomes are shown). In addition, the figure illustrates the essential edges (Section 2.6) of each bimodule. The resulting bipartite graph provides insight into the underlying associations between SNPs and genes that constitute the bimodule. See Appendix C.8 for more such illustrations.

4.3.3 GENE ONTOLOGY ENRICHMENT FOR BIMODULES

The Gene Ontology (GO) database contains a curated collection of gene sets that are known to be associated with different biological functions (c.f. Gene Ontology Consortium, 2014; Botstein et al., 2000; Rhee et al., 2008). The topGO (Alexa and Rahnenfuhrer, 2018) package assesses whether sets in the GO database are enriched for a given gene set using Fisher’s test. For each of the 145 BSP bimodules having a gene set B with 8 or more

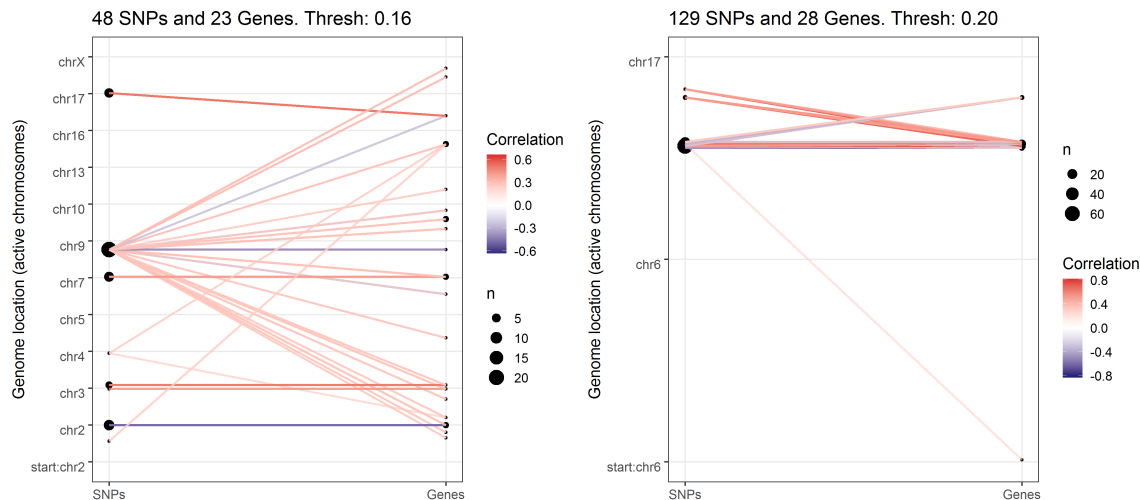


Figure 5: The gene-SNP association network for two BSP bimodules mapped onto the genome. The network of *essential edges* was formed by thresholding the cross-correlation matrix for the bimodule at the connectivity threshold (Section 2.6).

elements, we used topGO to assess the enrichment of B in 6463 GO gene sets of size more than 10, representing biological processes. We retained results with significant BH q -values ($\alpha = .05$). Of the 145 gene sets considered, 18 had significant overlap with one or more biological process, though these processes did not appear to be related to thyroid-specific function. Repeating with randomly chosen gene sets of the same size yielded no results. The significant GO terms for BSP and CONDOR can be found in Appendix C.9.

5. Application of BSP to North American Temperature and Precipitation Data

5.1 Introduction

The relationship between temperature and precipitation over North America has been well documented (Madden and Williams, 1978; Berg et al., 2015; Adler et al., 2008; Livneh and Hoerling, 2016; Hao et al., 2018) and is of agricultural importance. For example, Berg et al. (2015) noted widespread correlation between summertime mean temperature and precipitation at the same location over various land regions. We explore these relationships using the Bimodule Search Procedure. In particular, the method allows us to search for clusters of distal temperature-precipitation relationships, known as teleconnections, whereas previous work has mostly focused on analyzing spatially proximal correlations.

We applied BSP to find pairs of geographic regions such that summer temperature in the first region is significantly correlated in aggregate with summer precipitation in the second region one year later. We will refer to such region pairs as T-P (temperature-precipitation) bimodules. T-P bimodules reflect mesoscale analysis of region-specific climatic patterns,

which can be useful for predicting impact of climatic changes on practical outcomes like agricultural output.

5.2 Data Description and Processing

The Climatic Research Unit (CRU TS version 4.01) data (Harris et al., 2014) contains daily global measurements of temperature (T) and precipitation (P) levels on land over a $.5^\circ \times .5^\circ$ (360 pixels by 720 pixels) resolution grid from 1901 to 2016. We reduced the resolution of the data to $2.5^\circ \times 2.5^\circ$ (72 by 144 pixels) by averaging over neighboring pixels and restricted to 427 pixels corresponding to the latitude-longitude pairs within North America. For each available year and each pixel/location we averaged temperature (T) and precipitation (P) over the summer months of June, July, and August. Each feature of the resulting time series was centered and scaled to have zero mean and unit variance. The data matrix \mathbb{X} , reflecting temperature, had 115 rows containing the annual summer-aggregated temperatures from 1901 to 2015 for each of the 427 locations. The data matrix \mathbb{Y} , reflecting precipitation, had 115 rows containing the annual summer-aggregated precipitation from 1902 to 2016 (lagged by one year from temperature) for each of the 427 locations.

Analysis of summer precipitation versus summer temperatures lagged by 2 years, and temperatures from different seasons (winter T; summer P of the same year) in the same year did not yield any bimodules.

5.3 Bimodules Search Procedure and Diagnostics

We applied BSP on the climate data with the false discovery parameter $\alpha = 0.045$, selected using the procedure in Appendix C.4, to keep edge-error under 0.1 (see Figure 13, Appendix D). BSP searches for groups of temperature and precipitation pixels that have significant aggregate cross-correlation. Temperature and precipitation data exhibit both spatial and temporal auto-correlations. The BSP procedure does not make use of the pixel locations. While the permutation null employed by BSP directly accounts for spatial-correlations within the temperature and the precipitation data, we note that it does not directly account for temporal correlations, which violate a sample exchangeability assumption used in the p-value approximations. The temporal auto-correlation in our data was moderate, ranging from 0.10 to 0.30 for various features.

BSP found five distinct bimodules; the effective number of bimodules was three. After filtering, the two bimodules illustrated in Figure 6 and another bimodule with 80 temperature pixels and 5 precipitation pixels remained. We omitted a further analysis of the third bimodule as its precipitation pixels were same as those of Bimodule 2 in Figure 6 and its temperature pixels were geographically scattered.

Temperature pixels in Bimodules 1 and 2 are situated distally from the precipitation pixels, but the temperature and precipitation pixels within each bimodule form blocks of contiguous geographical regions. Since BSP did not make use of any location information when searching for bimodules, these effects might have a common spatial origin.

The locations regions identified by the bimodules occupy large geographical areas. The precipitation pixels from Bimodule 1 form a vertical stretch around the eastern edge of the Great Plains and are correlated with temperature pixels in large areas of the Pacific Northwest, Alaska, and Mexico. In Bimodule 2 precipitation in the southern Great Plains

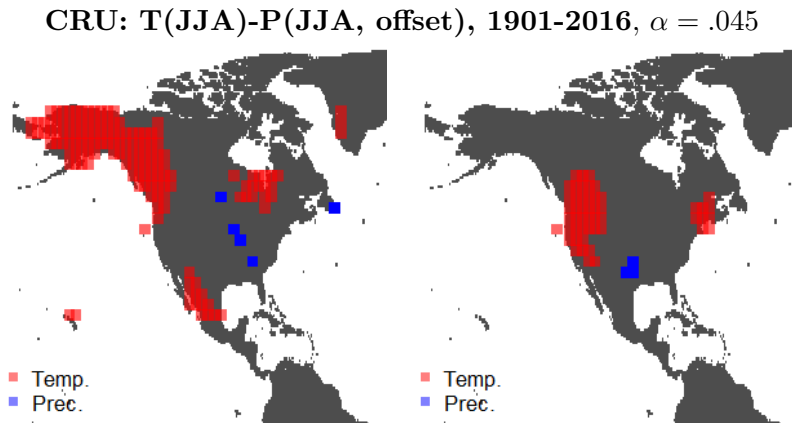


Figure 6: Bimodules of summer temperature and precipitation in North America from CRU observations from 1901-2016. The left bimodule (1) contains 149 temperature locations (pixels) and 6 precipitation locations. The right bimodule (2) contains 53 temperature and 5 precipitation locations.

around Oklahoma is strongly correlated with temperature in the Northwestern Great Plains. An anomalously hot summer Oregon in one year in the Northwest suggests an anomalously rainy growing season in the following year in the Southern Great Plains. Pixel-wise positive correlations are discussed in Appendix D.

The coastal proximity of all the temperature clusters suggest influences of oscillations in sea surface temperatures. Aforementioned patterns from both bimodules map to locations of agricultural productivity, such as in Oklahoma and Missouri (Figure 6).

The bimodules found by BSP only consider the magnitudes of correlations between temperature and precipitation. Further analysis of these bimodules shows that the significant correlations between temperature and precipitation are positive in the Great Plains region. These results agree with findings on concurrent T-P correlations in the Great Plains (Zhao and Khalil, 1993; Berg et al., 2015; Wang et al., 2019), which noted widespread correlations between summertime mean temperatures and precipitation at the same location over land in various parts of North America, notably the Great plains. Our findings show strong correlations between northwestern (coastal) temperatures and Great Plains precipitation and generally agree with findings in the literature. For example, Livneh and Hoerling (2016) considered the relationship between hot temperatures and droughts in the Great Plains, noting that hot temperatures in the summer are related to droughts in the following year on the overall global scale. The results of Livneh and Hoerling (2016) preface the results contained within the above bimodules, but the latter are additionally able to find regions where this effect is significant.

Our findings demonstrate the utility of BSP in finding insights into remote correlations between precipitation and temperature in North America. Further research may build on these exploratory findings and create a model that can forecast precipitation in agriculturally productive regions around the world.

6. Discussion

The Bimodule Search Procedure (BSP) is an exploratory tool that searches for groups of features with significant aggregate cross-correlation, which we refer to as bimodules. Rather than relying on an underlying generative model, BSP makes use of iterative hypothesis-testing to identify stable bimodules, which satisfy a natural stability condition. The false discovery threshold $\alpha \in (0, 1)$ is the only free parameter of the procedure. Efficient approximation of the p-values used for iterative testing allow BSP to run on large datasets.

Using a complex, network-based simulation study, we found that BSP was able to recover most target bimodules with significant cross-correlation strength, while simultaneously controlling the false discovery of edges having network-level importance. Among target bimodules with similar cross-correlation strengths, those with lower intra-correlations were more likely to be recovered than those with higher intra-correlations, reflecting the incorporation of intra-correlations in the calculation of p-values; the effects of intra-correlations were most pronounced when the cross-correlation strength was moderate.

When applied to eQTL data, BSP bimodules identified both local and distal effects, capturing half of the eQTLs found by standard cis-analysis and most of the eQTLs found by standard trans-analysis. Further, a substantial proportion of bimodules contained SNP-gene pairs that were important at the network level but not deemed significant under the standard (pairwise) eQTL-analysis.

At root, the discovery of bimodules by BSP and CONDOR is driven by the presence or absence of correlations between features of different types. A key issue for these, and related, methods is how they behave with increasing sample size. In general, increasing sample size will yield greater power to detect cross-correlations, and therefore one expects the sizes of bimodule to increase. While this is often a desirable outcome, in applications where non-zero cross-correlations (possibly of small size) are the norm, this increased power may yield very large bimodules with little interpretive value. Evidence of this phenomena is found in the simulation study where, due to the presence of confounding edges between target bimodules, increasing the sample size from $n = 200$ to $n = 600$ yields larger BSP bimodules, which often contain multiple target bimodules (Appendix B.3). This may well reflect the underlying biology of genetic regulation: the omni-genic hypothesis of Boyle et al. (2017) suggests that a substantial portion of the gene-SNP cross-correlation network might be connected at the population level.

An obvious way to address “super connectivity” of the cross-correlation network is to change the definition of bimodule to account for the magnitude of cross-correlations, rather than their mere presence or absence. Incorporating a more stringent definition of connectivity in BSP would require modifying the permutation null distribution and addressing the theory and computation behind such a modification, both of which are areas of future research.

SUPPLEMENTARY MATERIAL

Appendix: The appendix section below contains further details on BSP implementation (Section A), simulation study (Section B), eQTL analysis (Section C), and the climate analysis (Section D).

BSP software: <https://github.com/miheerdew/cbce>

Acknowledgment

M.D., J.P., and A.B.N. were supported by NIH grant R01 HG009125-01 and NSF grants DMS-1613072 and DMS-2113676. A.B.N. was also supported by NSF Grant DMS 2113676. M.H. was awarded the Department of Defense, Air Force Office of Scientific Research, National Defense Science and Engineering Graduate (NDSEG) Fellowship, 32 CFR 168a and funded by government support under contract FA9550-11-C-0028. M.I.L. was supported by NIH grants R01 HG009125-01 and R01-HG009937. The authors wish to acknowledge numerous helpful conversations with Professors Fred Wright and Richard Smith.

References

- Robert F. Adler, Guojun Gu, Jian-Jian Wang, George J. Huffman, Scott Curtis, and David Bolvin. Relationships between global precipitation and surface temperature on interannual and longer timescales (1979–2006). *Journal of Geophysical Research: Atmospheres*, 113(D22), 2008.
- Frank W Albert and Leonid Kruglyak. The role of regulatory variation in complex traits and disease. *Nature Reviews Genetics*, 16(4):197, 2015.
- Adrian Alexa and Jorg Rahnenfuhrer. *topGO: Enrichment Analysis for Gene Ontology*, 2018. R package version 2.34.0.
- Michael J Barber. Modularity and community detection in bipartite networks. *Physical Review E*, 76(6):066102, 2007.
- Stephen J Beckett. Improved community detection in weighted bipartite networks. *Royal Society open science*, 3(1):140536, 2016.
- Yoav Benjamini and Yosef Hochberg. Controlling the false discovery rate: a practical and powerful approach to multiple testing. *Journal of the Royal statistical society: series B (Methodological)*, 57(1):289–300, 1995.
- Yoav Benjamini and Daniel Yekutieli. The control of the false discovery rate in multiple testing under dependency. *Annals of Statistics*, 29(4):1165–1188, 08 2001.
- Alexis Berg, Benjamin R. Lintner, Kirsten Findell, Sonia I. Seneviratne, Bart van den Hurk, Agnès Ducharne, Frédérique Chéry, Stefan Hagemann, David M. Lawrence, Sergey Malyshev, Arndt Meier, and Pierre Gentine. Interannual coupling between summertime surface temperature and precipitation over land: Processes and implications for climate change. *Journal of Climate*, 28(3):1308–1328, 2015.
- Kelly Bodwin, Kai Zhang, Andrew Nobel, et al. A testing based approach to the discovery of differentially correlated variable sets. *The Annals of Applied Statistics*, 12(2):1180–1203, 2018.

- Béla Bollobás. The evolution of random graphs—the giant component. In *Random graphs*, volume 184, pages 130–59. Cambridge university press Cambridge, 2001.
- David Botstein, J Ms Cherry, M Ashburner, CA Ball, JA Blake, H Butler, AP Davis, K Dolinski, SS Dwight, JT Eppig, et al. Gene ontology: tool for the unification of biology. *Nat genet*, 25(1):25–9, 2000.
- Evan A Boyle, Yang I Li, and Jonathan K Pritchard. An expanded view of complex traits: from polygenic to omnigenic. *Cell*, 169(7):1177–1186, 2017.
- Aravinda Chakravarti and Tychele N Turner. Revealing rate-limiting steps in complex disease biology: The crucial importance of studying rare, extreme-phenotype families. *BioEssays*, 38(6):578–586, 2016.
- Jun Chen, Frederic D Bushman, James D Lewis, Gary D Wu, and Hongzhe Li. Structure-constrained sparse canonical correlation analysis with an application to microbiome data analysis. *Biostatistics*, 14(2):244–258, 2013.
- Xiaohui Chen, Xinghua Shi, Xing Xu, Zhiyong Wang, Ryan Mills, Charles Lee, and Jinbo Xu. A two-graph guided multi-task lasso approach for eqtl mapping. *Journal of Machine Learning Research*, 22:208–217, 2012.
- Wei Cheng, Xiang Zhang, Yubao Wu, Xiaolin Yin, Jing Li, David Heckerman, and Wei Wang. Inferring novel associations between snp sets and gene sets in eqtl study using sparse graphical model. In *Proceedings of the ACM Conference on Bioinformatics, Computational Biology and Biomedicine*, pages 466–473. ACM, 2012.
- Wei Cheng, Yu Shi, Xiang Zhang, and Wei Wang. Fast and robust group-wise eqtl mapping using sparse graphical models. *BMC bioinformatics*, 16(1):2, 2015.
- Wei Cheng, Yu Shi, Xiang Zhang, and Wei Wang. Sparse regression models for unraveling group and individual associations in eqtl mapping. *BMC bioinformatics*, 17(1):136, 2016.
- Alberto Costa and Pierre Hansen. A locally optimal hierarchical divisive heuristic for bipartite modularity maximization. *Optimization letters*, 8(3):903–917, 2014.
- Miheer Dewaskar and Andrew B. Nobel. Large sample analysis of the bimodule search procedure. (*in preparation*), 2022.
- Stéphane Dray, Daniel Chessel, and Jean Thioulouse. Co-inertia analysis and the linking of ecological data tables. *Ecology*, 84(11):3078–3089, 2003.
- Maud Fagny, Joseph N Paulson, Marieke L Kuijjer, Abhijeet R Sonawane, Cho-Yi Chen, Camila M Lopes-Ramos, Kimberly Glass, John Quackenbush, and John Platig. Exploring regulation in tissues with eqtl networks. *Proceedings of the National Academy of Sciences*, 114(37):E7841–E7850, 2017.
- Gene Ontology Consortium. Gene ontology consortium: going forward. *Nucleic acids research*, 43(D1):D1049–D1056, 2014.

- GTEEx Consortium. Genetic effects on gene expression across human tissues. *Nature*, 550 (7675):204, 2017.
- Zengchao Hao, Fanghua Hao, Vijay P. Singh, and Xuan Zhang. Quantifying the relationship between compound dry and hot events and el niño–southern oscillation (enso) at the global scale. *Journal of Hydrology*, 567:332 – 338, 2018. ISSN 0022-1694.
- I. Harris, P.D. Jones, T.J. Osborn, and D.H. Lister. Updated high-resolution grids of monthly climatic observations – the cru ts3.10 dataset. *International Journal of Climatology*, 34(3):623–642, 2014.
- Yang Huang, Stefan Wuchty, Michael T Ferdig, and Teresa M Przytycka. Graph theoretical approach to study eqtl: a case study of plasmodium falciparum. *Bioinformatics*, 25(12): i15–i20, 2009.
- Liis Kolberg, Nurlan Kerimov, Hedi Peterson, and Kaur Alasoo. Co-expression analysis reveals interpretable gene modules controlled by *trans*-acting genetic variants. *eLife*, 9: e58705, sep 2020. ISSN 2050-084X.
- D. Lahat, T. Adali, and C. Jutten. Multimodal data fusion: An overview of methods, challenges, and prospects. *Proceedings of the IEEE*, 103(9):1449–1477, 2015.
- Xin Liu and Tsuyoshi Murata. An efficient algorithm for optimizing bipartite modularity in bipartite networks. *Journal of Advanced Computational Intelligence and Intelligent Informatics*, 14(4):408–415, 2010.
- Ben Livneh and Martin P. Hoerling. The physics of drought in the u.s. central great plains. *Journal of Climate*, 29(18):6783–6804, 2016.
- Roland A. Madden and Jill Williams. The correlation between temperature and precipitation in the united states and europe. *Monthly Weather Review*, 106(1):142–147, 1978.
- Sean D McCabe, Dan-Yu Lin, and Michael I Love. Consistency and overfitting of multi-omics methods on experimental data. *Brief Bioinform*, 2019.
- AR McIntosh, FL Bookstein, James V Haxby, and CL Grady. Spatial pattern analysis of functional brain images using partial least squares. *Neuroimage*, 3(3):143–157, 1996.
- Chen Meng, Oana A Zeleznik, Gerhard G Thallinger, Bernhard Kuster, Amin M Gholami, and Aedín C Culhane. Dimension reduction techniques for the integrative analysis of multi-omics data. *Briefings in bioinformatics*, 17(4):628–641, 2016.
- Carson Mosso, Kelly Bodwin, Suman Chakraborty, Kai Zhang, and Andrew B Nobel. Latent association mining in binary data. *arXiv preprint arXiv:1711.10427*, 2017.
- Alexandra C Nica and Emmanouil T Dermitzakis. Expression quantitative trait loci: present and future. *Philosophical Transactions of the Royal Society B: Biological Sciences*, 368(1620):20120362, 2013.

- John Palowitch, Shankar Bhamidi, and Andrew B Nobel. The continuous configuration model: A null for community detection on weighted networks. *arXiv preprint arXiv:1601.05630*, 2016.
- Chu Pan, Jiawei Luo, Jiao Zhang, and Xin Li. BiModule: biclique modularity strategy for identifying transcription factor and microRNA co-regulatory modules. *IEEE/ACM Transactions on Computational Biology and Bioinformatics*, 2019. ISSN 1545-5963, 1557-9964, 2374-0043.
- Elena Parkhomenko, David Tritchler, and Joseph Beyene. Sparse canonical correlation analysis with application to genomic data integration. *Statistical applications in genetics and molecular biology*, 8(1), 2009.
- P. V. Patel, T. A. Gianoulis, R. D. Bjornson, K. Y. Yip, D. M. Engelman, and M. B. Gerstein. Analysis of membrane proteins in metagenomics: Networks of correlated environmental features and protein families. *Genome Research*, 20(7):960–971, July 2010. ISSN 1088-9051.
- Paola Pesantez-Cabrera and Ananth Kalyanaraman. Detecting communities in biological bipartite networks. In *Proceedings of the 7th ACM International Conference on Bioinformatics, Computational Biology, and Health Informatics*, pages 98–107, 2016.
- John Platig. *condor: COmplex Network Description Of Regulators*, 2016. R package.
- John Platig, Peter J Castaldi, Dawn DeMeo, and John Quackenbush. Bipartite community structure of eqtls. *PLoS computational biology*, 12(9):e1005033, 2016.
- Bettina M Pucher, Oana A Zeleznik, and Gerhard G Thallinger. Comparison and evaluation of integrative methods for the analysis of multilevel omics data: a study based on simulated and experimental cancer data. *Briefings in bioinformatics*, 20(2):671–681, 2019.
- Seung Yon Rhee, Valerie Wood, Kara Dolinski, and Sorin Draghici. Use and misuse of the gene ontology annotations. *Nature Reviews Genetics*, 9(7):509–515, 2008.
- Kris Sankaran and Susan P Holmes. Multitable methods for microbiome data integration. *Frontiers in genetics*, 10, 2019.
- Andrey A Shabalin. Matrix eqtl: ultra fast eqtl analysis via large matrix operations. *Bioinformatics*, 28(10):1353–1358, 2012.
- Andrey A Shabalin, Victor J Weigman, Charles M Perou, Andrew B Nobel, et al. Finding large average submatrices in high dimensional data. *The Annals of Applied Statistics*, 3(3):985–1012, 2009.
- Lu Tian, Andrew Quitadamo, Frederick Lin, and Xinghua Shi. Methods for population-based eqtl analysis in human genetics. *Tsinghua Science and Technology*, 19(6):624–634, 2014.

- Giulia Tini, Luca Marchetti, Corrado Priami, and Marie-Pier Scott-Boyer. Multi-omics integration—a comparison of unsupervised clustering methodologies. *Briefings in bioinformatics*, 20(4):1269–1279, 2019.
- Sandra Waaijenborg, Philip C Verselewele de Witt Hamer, and Aeilko H Zwinderman. Quantifying the association between gene expressions and dna-markers by penalized canonical correlation analysis. *Statistical applications in genetics and molecular biology*, 7(1), 2008.
- Bin Wang, Xiao Luo, Young-Min Yang, Weiyi Sun, Mark A. Cane, Wenju Cai, Sang-Wook Yeh, and Jian Liu. Historical change of el niño properties sheds light on future changes of extreme el niño. *Proceedings of the National Academy of Sciences*, 116(45):22512–22517, 2019. ISSN 0027-8424.
- Harm-Jan Westra and Lude Franke. From genome to function by studying eqtls. *Biochimica et Biophysica Acta (BBA)-Molecular Basis of Disease*, 1842(10):1896–1902, 2014.
- James D Wilson, Simi Wang, Peter J Mucha, Shankar Bhamidi, Andrew B Nobel, et al. A testing based extraction algorithm for identifying significant communities in networks. *The Annals of Applied Statistics*, 8(3):1853–1891, 2014.
- Anderson M Winkler, Olivier Renaud, Stephen M Smith, and Thomas E Nichols. Permutation inference for canonical correlation analysis. *Neuroimage*, 220:117065, 2020.
- Daniela Witten and Rob Tibshirani. *PMA: Penalized Multivariate Analysis*, 2020. URL <https://CRAN.R-project.org/package=PMA>. R package version 1.2.1.
- Daniela M Witten, Robert Tibshirani, and Trevor Hastie. A penalized matrix decomposition, with applications to sparse principal components and canonical correlation analysis. *Biostatistics*, 10(3):515–534, 2009.
- Xuebing Wu, Qifang Liu, and Rui Jiang. Align human interactome with phenome to identify causative genes and networks underlying disease families. *Bioinformatics*, 25(1):98–104, January 2009. ISSN 1367-4803. Publisher: Oxford Academic.
- Weining Zhao and M. A. K. Khalil. The relationship between precipitation and temperature over the contiguous united states. *Journal of Climate*, 6(6):1232–1236, 1993.
- Xiuwen Zheng. *A Tutorial for the R/Bioconductor Package SNPRelate*, 2015.
- Yi-Hui Zhou, William T Barry, and Fred A Wright. Empirical pathway analysis, without permutation. *Biostatistics*, 14(3):573–585, 2013.
- Yi-Hui Zhou, Paul Gallins, and Fred Wright. Marker-trait complete analysis. *bioRxiv*, page 836494, 2019.

A. BSP implementation details

A.1 Dealing with cycles and large sets

In practice, we do not want the sizes of the sets (A_k, B_k) in the iteration to grow too large as this slows computation, and large bimodules are difficult to interpret. Therefore the search procedure is terminated when the geometric size of (A_k, B_k) exceeds 5000. In some cases, the sequence of iterates (A_k, B_k) for $k \in \{1, \dots, k_{max}\}$ will form a cycle of length greater than 1, and will therefore fail to reach a fixed point. To search for a nearby fixed point instead, when we encounter the cycle $(A_k, B_k) = (A_l, B_l)$ for some $l < k - 1$, we set (A_{l+1}, B_{l+1}) to $(A_k \cap A_{k-1}, B_k \cap B_{k-1})$ and continue the iteration.

A.2 Initialization heuristics for BSP

In practice, BSP is initialized with each singleton pair $(\{s\}, \emptyset)$ for $s \in S$, and each singleton pair $(\emptyset, \{t\})$ for $t \in T$. When either of the sets S or T is large, we use additional strategies to speed up computation. When $|S| \gg |T|$, we initialize BSP from all the features in T , but only from a subset of randomly chosen features in S .

BSP sometimes discovers identical or almost-identical bimodules when starting from different initializations, often from features within the said bimodule. This problem is particularly prominent for large bimodules which may be rediscovered by thousands of initializations. Hence, to avoid some of this redundant computation, we provide an option to skip initializing BSP from features in the bimodules that have already been discovered. This option was not however used for the examples in this paper.

A.3 Choice of α using half-permutation based edge-error estimates

To select the false discovery parameter α for BSP, we estimate the *edge-error* for each value of α from a pre-specified grid. The edge-error is an edge-based false discovery notion for bimodules, defined as the average fraction of erroneous essential-edges (defined in Section 2.6) among bimodules. Since we do not know the ground truth, we estimate the edge-error for BSP by running it on instances of the *half-permuted* dataset in which the sample labels for half of the features from each data type have been permuted. Further details are given below.

A.3.1 HALF-PERMUTATION

Comparing results between the original and permuted data (Definition 1) allow us to assess the false discoveries from BSP when there are no true associations between features from S and T . However, we often expect associations between at least some variables from S and T (in fact, these are the ones that we want to find). To create a null distribution where some pairs of features from S and T are correlated and some are not, we use the following half-permutation scheme. Let (\mathbb{X}, \mathbb{Y}) denote the original data, where \mathbb{X} and \mathbb{Y} are measurements matrices for the two data types. We generate a *half-permuted* dataset $(\tilde{\mathbb{X}}, \tilde{\mathbb{Y}})$ as follows:

1. Randomly select half the features, $\hat{S} \subseteq S$ and $\hat{T} \subseteq T$, from each data type.

2. Randomly permute the rows of the submatrix of \mathbb{X} that corresponding to the columns \hat{S} , and call the resulting matrix $\tilde{\mathbb{X}}$. In other words, the submatrix corresponding to the features $S \setminus \hat{S}$ is the same in \mathbb{X} and $\tilde{\mathbb{X}}$, while the sample labels of the submatrix of $\tilde{\mathbb{X}}$ corresponding to features in \hat{S} have been permuted $\mathbb{X}_{\hat{S}} = \mathbf{P}_1 \mathbb{X}_{\hat{S}}$ by a random permutation matrix \mathbf{P}_1 .
3. Similarly, permute the rows of matrix \mathbb{Y} corresponding to the features \hat{T} using another independent permutation matrix \mathbf{P}_2 . Call the resulting matrix $\tilde{\mathbb{Y}}$.

Note that, together, the ‘‘half-permutation’’ steps 2 and 3 temper the cross-correlation between pairs of features in $\hat{S} \times T \cup S \times \hat{T}$. Let $\mathcal{B} = \{(A_1, B_1), (A_2, B_2) \dots (A_K, B_K)\}$ be the collection of bimodules in the half-permuted data $(\tilde{\mathbb{X}}, \tilde{\mathbb{Y}})$. We will assume that the collection \mathcal{B} is already filtered for overlaps (see Section 2.5). We define the edge-error estimate for the collection \mathcal{B} as

$$\widehat{\text{edge-error}}(\mathcal{B}) = \frac{1}{|\mathcal{B}|} \sum_{(A,B) \in \mathcal{B}} \frac{|\text{essential-edges}(A, B) \cap (\hat{S} \times T \cup S \times \hat{T})|}{|\text{essential-edges}(A, B)|}. \quad (7)$$

In practice, we generate half-permuted datasets and use the edge-error estimate (7) to choose α as follows. First, we generate a pre-specified number N of instances of the half-permuted dataset. If the covariates are present, we correct for them after the half-permutation step. Next, for each α among a range of values, e.g. $\{0.01, 0.02, \dots, 0.05\}$, we run BSP with false discovery parameter α over the each of the half-permuted datasets and calculate the average edge-error (7) of the resulting collection of bimodules for that value of α , averaged over all the N half-permuted instances. We can then choose an α from the grid that has average edge-error smaller a pre-specified value like 0.05. Generally smaller values of α tend to have smaller edge error, so we choose the largest value of α from the grid that has acceptable edge error. However, we may also chose a smaller value of α if the bimodules are too large.

A caveat with the above procedure to select α is that the edge-error estimates may be quite variable even when averaged over a large number N of half-permuted datasets. One explanation for this variability is that different \hat{S} and \hat{T} are chosen for each instance of the half-permutation. Nevertheless, if we observe variability we choose a more conservative value of α . As seen in Section B.2.1, even without access to the ground truth, we were able to keep the true edge-error under 0.05 by using the above strategy to select α .

A.4 Covariate correction

In some cases the data matrices $[\mathbb{X}, \mathbb{Y}] \in \mathbb{R}^{n \times (p+q)}$ are accompanied by one or more covariates like sex, platform details and PEER factors that must be accounted for by removing their effects before discovering bimodules. Suppose we are given m such linearly independent covariates $v_1, \dots, v_m \in \mathbb{R}^n$. Here we describe how to modify BSP to remove their effects. First, we residualize each column of the original data $[\mathbb{X}, \mathbb{Y}]$ by setting up a linear model with explanatory variables v_1, \dots, v_m . Denote the resulting matrix by $[\mathbb{X}', \mathbb{Y}'] \in \mathbb{R}^{n \times (p+q)}$ that has columns which are projections of those of $[\mathbb{X}, \mathbb{Y}]$ onto the subspace orthogonal to v_1, \dots, v_m . We would like to now run BSP on $[\mathbb{X}', \mathbb{Y}']$, however since the columns of $D' = [\mathbb{X}', \mathbb{Y}']$ lie on an

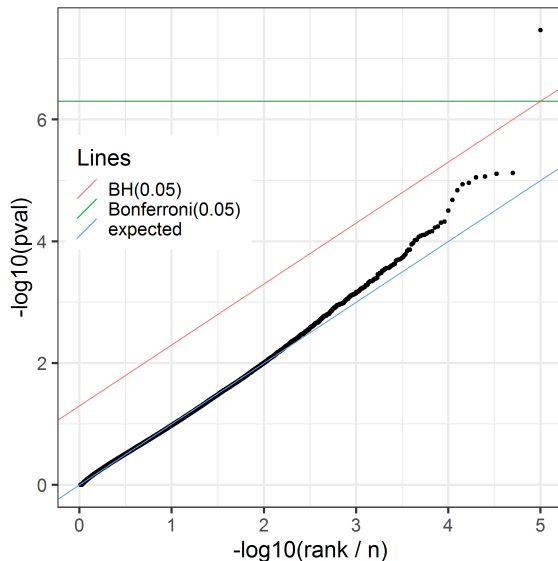


Figure 7: Assessing the accuracy of our p-value estimate $\hat{p}(A, t)$: We used the eQTL data from Section 4 and chose a bimodule with 24 SNPs (used as A) and selected t to be a gene from the same bimodule. We then performed 10^5 random permutation of the sample labels for the gene t and repeatedly estimated $\hat{p}(A, t)$ for each permutation after removing the effects of covariates (Appendix A.4).

$n' = n - m'$ dimensional subspace, the permutation p-values (Section 2.2) based on data D' will tend to be significant even if \mathbb{X} and \mathbb{Y} were generated independently. However following Zhou et al. (2013), the eigenvalue-conditional p-value approximation can be corrected by replacing the sample size n with the effective sample size of n' in the moment calculations.

A.5 Uniformity of our p-value estimates

For a quick check of the uniformity of our p-value approximation under the permutation null, we chose a bimodule (A, B) found in Section 4 and a $t \in B$. Then we randomly permuted the labels of gene t (10^5 times), computing our estimate $\hat{p}(A, t)$ of the permutation p-value $p(A, t)$ (Section 2.2) in each case. Hence we are assessing the uniformity of $\hat{p}(A, t)$ under the permutation null distribution. The result in Figure 7 shows that the computed p-values are almost uniform but extremely small p-values show anti-conservative behavior. A potential reason for this anti-conservative behavior is that the tails of test statistic under the permutation distribution may be heavier compared to the tails of the location-shifted Gamma distribution that we use to approximate it, since the permutation distribution is discrete distribution which explicitly depends on the exact entries of the data matrices.

B. Simulation study details

B.1 Details of the Simulated Data

We generated a single large dataset having $n = 200$ samples and two measurement types, with $p = 100,000$ and $q = 20,000$ features, respectively. The number of features is of the same order of magnitude as in the eQTL dataset considered in Section 4. Following the notation at the beginning of Section 2.1, we denote the two types of features by index sets $S = \{s_1, s_2 \dots s_p\}$ and $T = \{t_1, t_2 \dots t_q\}$. For each individual, the joint $p + q$ dimensional measurement vector is independently drawn from a multivariate normal distribution with mean $0 \in \mathbb{R}^{p+q}$ and $(p + q) \times (p + q)$ covariance matrix Σ . The covariance matrix Σ is designed so that it has $K = 500$ target bimodules of various sizes, network structures, signal strengths and intra-correlations.

As it is difficult to generate structured covariance matrices while maintaining non-negative definiteness, we instead specify a generative model for the $p + q$ dimensional random row vector $(X, Y) \sim \mathcal{N}_{p+q}(0, \Sigma)$. To begin, we partitioned the first-half of the S -indices $\{s_1, \dots, s_{\lceil p/2 \rceil}\}$ into K disjoint subsets A_1, A_2, \dots, A_K with sizes chosen according to a Dirichlet distribution with parameter $(1, 1, \dots, 1) \in \mathbb{R}^K$. In the same way, we generated a Dirichlet partition B_1, B_2, \dots, B_K of the first-half of T indices $\{t_1, \dots, t_{\lceil q/2 \rceil}\}$ independent of the previous partition. The feature-set pairs (A_i, B_i) constitute the target bimodules, while the features in second-half of the S - and T -indices are not part of target bimodules. Next, the random sub-vectors (X_{A_i}, Y_{B_i}) corresponding to the target bimodules were generated independently for each $i \in [K]$ using a graph based regression model described below.

Let (A, B) be a feature set pair, and suppose that $\rho \in [0, 1)$ and $\sigma^2 > 0$ are given. Let $D \in \{0, 1\}^{|A| \times |B|}$ be a binary matrix, which we regard as the adjacency matrix of a connected bipartite network with vertex set $A \cup B$. Then the random row-vector (X_A, Y_B) is generated as follows:

$$X_A \sim \mathcal{N}_{|A|}(0, (1 - \rho)I + \rho U) \quad \text{and} \quad Y_B = X_A D + \epsilon, \quad (8)$$

where $\epsilon \sim \mathcal{N}_{|B|}(0, \sigma^2 I)$ and U is a matrix of all ones. To understand the bimodule signal produced by this model, note that ρ governs the intra-correlation between features in A and that for any $t \in B$, the variable Y_t is influenced by features X_s such that (s, t) is an edge in the adjacency matrix D . For each of the target bimodules (A_i, B_i) in the simulation, we independently chose parameters ρ_i , σ_i^2 , and D_i to produce a variety of behaviors while maintaining the inherent constraints between them (further details are described in Section B.4.1 below).

Features X_{s_j} with $j > \lceil p/2 \rceil$ are independent $\mathcal{N}(0, 1)$ noise variables. Features Y_{t_r} with $r > \lceil q/2 \rceil$ are either noise (standard normal) or they are bridge variables that connect two target bimodules. In more detail, for every pair of distinct bimodules (A_k, B_k) and (A_l, B_l) with $1 \leq k < l \leq K$, with probability $q = \frac{1.5}{K}$, we connect the two bimodules by selecting at random (and without replacement) an index $r > \lceil q/2 \rceil$ and making it a bridge variable by defining

$$Y_{t_r} = X_s + X_{s'} + \epsilon \quad \text{with} \quad \epsilon \sim N(0, \sigma_r^2), \quad (9)$$

for a randomly chosen $s \in A_k$ and $s' \in A_l$. The noise variance σ_r^2 in (9) is chosen so that the correlation between Y_{t_r} and X_s (and $X_{s'}$) is equal to the average of the maximum

correlation of the bimodules that are being connected. If Y_{t_r} is not a bridge variable, it is taken to be noise (standard normal).

Prior to the addition of bridge variables, the connected components of the population cross-correlation network are just the bimodules (A_k, B_k) . Once bridge variables have been added, the population cross-correlation network will have a so-called giant connected component comprising a substantial portion of the underlying index space $S \times T$. While theoretical support for the presence of giant component in our simulation model comes from the study of Erdős-Renyi random graphs (Bollobás, 2001), such components have also been observed in empirical eQTL networks (Fagny et al., 2017; Platig et al., 2016). Since we only add a small number (348) of bridge variables, the majority of the cross-correlation signal is still contained in the more densely connected sets $\{(A_k, B_k)\}_{k=1}^K$.

B.2 Running BSP and Related Methods

We applied BSP to the simulated data using the false discovery parameter $\alpha = 0.01$, which was selected to keep the edge-error estimates under 0.05 (see Section A.3). This tuning procedure is purely based on the observed data, and does not use any knowledge of the ground truth. The search was initialized from singletons consisting of all the features in T and 1% of the features in S , chosen at random. In what follows, feature-set pairs identified by BSP (or some other method, when clear from context) will be referred to as *detected* bimodules. BSP detected 319 unique bimodules while the effective number (Section 2.5) of detected bimodules was 301.5.

To obtain bimodules via CONDOR (Platig et al., 2016), we applied Matrix-eQTL (Shabalin, 2012) to the simulated dataset with S considered as the set of SNPs and T considered as the set of genes, to extract feature pairs $(s, t) \in S \times T$ with q-value less than $\alpha = 0.05$. Next, we formed a bipartite graph on the vertex set $S \cup T$ with edges given by the significant feature pairs found in the previous step. The largest connected component of this graph, made up of 28,876 features from S and 6,455 features from T , was passed through a bipartite community detection software (Platig, 2016) which partitioned the nodes of the sub-graph into 112 bimodules.

We applied the sCCA method of Witten et al. (2009) to the simulated data to find 100 bimodules. More precisely, for various penalty parameters $\lambda \in [0, 1]$, we ran sCCA (Witten and Tibshirani, 2020) to find 100 canonical covariate pairs with the ℓ_1 norm constraint of $\lambda\sqrt{p}$ and $\lambda\sqrt{q}$ on the coefficients of the linear combinations corresponding to S and T respectively. Initially, we considered $\lambda = 0.233$, chosen by the permutation based procedure provided with the software. However the resulting bimodules were large and had high edge-error (further details are provided in Section B.4.2). Based on a rough grid search, we then ran the procedure with each value $\lambda \in \{.01, .02, .03, .04, .06\}$ to obtain smaller bimodules.

B.2.1 COMPARING PERFORMANCE OF THE METHODS

In the simulation study described above, we measure the recovery of a target bimodule (A_t, B_t) by a detected bimodule (A_d, B_d) using the two metrics:

$$\text{recall} = \frac{|A_t \cap A_d| |B_t \cap B_d|}{|A_t| |B_t|} \quad \text{and} \quad \text{Jaccard} = \frac{|A_t \cap A_d| |B_t \cap B_d|}{|(A_t \times B_t) \cup (A_d \times B_d)|}.$$

Recall captures how well the target bimodule is *contained* inside the detected bimodule, while Jaccard measures how well the two bimodules *match*. When assessing the recovery of a target bimodule under a collection of detected bimodules (like the output of BSP), we choose the detected bimodule with the best recall or Jaccard, depending on the metric under consideration.

As shown in Figure 2, the BSP Jaccard for target bimodules was influenced primarily by the cross-correlation strength $\sqrt{\frac{r^2(A,B)}{|A||B|}}$ of the target bimodule, though the intra-correlation parameter ρ used in the simulation (8) was also seen to have an effect (Figure 2, left). Most bimodules with cross-correlation strength above 0.4 were completely recovered, while those with strength below 0.2 were not recovered. For strengths between 0.2 to 0.4, there was a variation in Jaccard, with smaller Jaccard for bimodules having larger values of ρ (Figure 2, left). The effect of ρ on Jaccard was expected since BSP accounts for the intra-correlation among features of the same type.

The intra-correlation parameter ρ did not have significant effect on CONDOR Jaccard, since the method does not account for intra-correlations. Hence, here we only consider the effects of the cross-correlation strength of target bimodules on CONDOR Jaccard (Figure 2, green curve on the right). Regardless of the cross-correlation strength, CONDOR Jaccard remained low. This was because CONDOR bimodules often overlapped multiple target bimodules; indeed, 102 of the 112 CONDOR bimodules overlapped with two or more (up to 19) target bimodules, compared with only 21 of the 319 BSP bimodules. However, the results for CONDOR recall (Figure 2, purple curve on the right) show that most target bimodules with significant cross-correlation strengths were contained inside some CONDOR bimodule.

To assess the false discoveries in detected bimodules, we measured the *edge-error* of detected bimodules. The edge-error is the fraction of the essential-edges (Section 2.6) of a detected bimodule that are not part of the simulation model, that is, edges not contained in any target bimodule and not in the set of bridge edges. The average edge-error for BSP bimodules was 0.03, and 90% of the detected bimodules had edge-error under 0.05. In contrast, the average edge-error for CONDOR bimodules was 0.08, and 90% of the detected bimodules had edge-error under 0.14. The larger edge-error among CONDOR bimodules may have arisen because the method does not account for intra-correlations.

Concerning sCCA, the sizes of the detected bimodules were at least an order of magnitude larger than sizes of the target bimodules when λ exceeded 0.04 (see Figure 9 in Section B.4.2). Thus we only considered $\lambda \leq 0.04$. For $\lambda = 0.03$ and 0.04, the detected bimodules had large edge-error (average error 0.47 and 0.65, respectively), while for $\lambda = 0.01$ and 0.02 the target bimodules had poor recall (95% of the target bimodules had recall below 0.02 and 0.23, respectively). Further details of this results are given in Section B.4.2. A potential shortcoming of our application of sCCA was that we chose the same penalty parameter λ for each of the 100 bimodules. We expect that the results of sCCA would improve if one chose a different penalty parameter for each bimodule. However Witten et al. (2009) does not provide explicit guidelines to chose different penalty parameters for each component (bimodule), and directly doing a permutation-based grid search each time would be exceedingly slow.

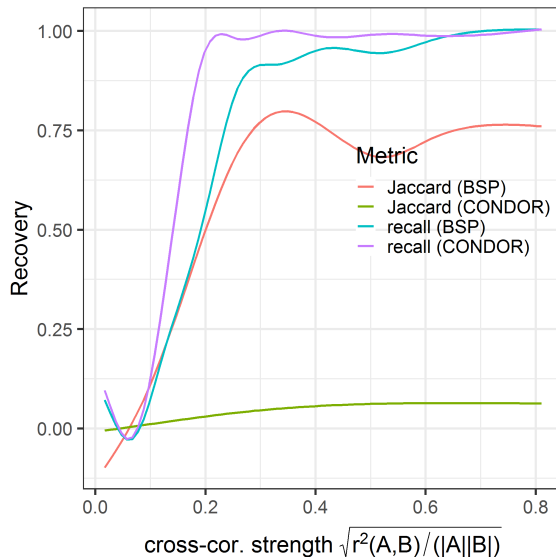


Figure 8: Average recall and Jaccard for target bimodules in the simulation with 600 samples.

B.3 Performance of BSP and CONDOR on increasing sample size

We also increased that sample size of the simulation study in the previous section to $n = 600$, and re-ran BSP and CONDOR with the same parameters as earlier. The average edge-error for BSP and CONDOR was 0.05 and 0.10 respectively. As seen in Figure 8, BSP and CONDOR both recall most bimodules with cross-correlation strength above 0.3, however Jaccard for BSP and CONDOR has degraded. This can be explained by noting that 25% of BSP bimodules now overlapped with two or more target bimodules compared to 6% when $n = 200$.

B.4 Further details of the simulation study

Here we provide more details of the simulation study that were briefly mentioned in Section B.1 and Section B.2.

B.4.1 SIMULATION MODEL FOR EACH TARGET BIMODULE

As described in Section B.1, given $\rho, \sigma \in [0, 1]$ and a binary adjacency matrix $D \in \{0, 1\}^{|A| \times |B|}$ representing a connected bipartite graph on vertices A and B (called the regressor-graph), the variables (X_A, Y_A) for a bimodule (A, B) can be simulated as

$$X_A \sim \mathcal{N}_{|A|}(0, (1 - \rho)I + \rho U) \quad \text{and} \quad Y_B^t = D^t X_A^t + \epsilon, \quad (10)$$

where U is the matrix of all ones and $\epsilon \sim N(0, \sigma^2)$. The parameters $\rho, \sigma \in [0, 1]$ and D appearing in (10) are chosen independently for each target bimodule (A, B) as follows:

1. Choose a constant $\beta \in [0, 1]$ uniformly at random. With $d \doteq \lceil \beta |A| \rceil$, let D be the adjacency matrix of the d -regular bipartite connected graph on vertex sets A and B

formed by independently connecting each vertex $t \in B$ to d randomly chosen vertices from A . If the resulting graph is not connected, set β to $\beta + \Delta\beta$ where $\Delta\beta = 0.1$ and repeat the previous step till the resulting bipartite graph is connected.

2. Randomly choose $\rho \in [0, 1]$ and $\eta \in [0, .8]$ subject to the constraint $\delta \doteq 1 + \rho(d - 1) \geq \eta^2 d$. We satisfy this constraint by first uniformly generating ρ and then generating η uniformly from $[0, \min(\sqrt{\delta d^{-1}}, .8)]$.
3. Finally let $\sigma = \frac{\sqrt{\delta(\delta - \eta^2 d)}}{\eta}$.

The constants (ρ, β, η) in the above procedure have the following intuitive role: ρ is the intra-correlation between any two features from the set A , $\beta \in [0, 1]$ controls the edge density of the regressor-graph D , and η is the cross-correlation between features from B and adjacent features from A in the regressor-graph. The following Lemma shows that our choice of parameters indeed results in population cross-correlation of η between features connected by the regressor-graph:

Lemma 5 *Fix $\rho, \eta \in [0, 1]$, $a, b \in \mathbb{N}$ and $d \in \{1, 2, \dots, a\}$ so that $\delta \doteq 1 + \rho(d - 1) \geq \eta^2 d$. Suppose \mathbf{X} is an a -dimensional random vector with covariance matrix $\text{Cov}(\mathbf{X}) = \rho U_a + (1 - \rho)I_a$, where $U_a \in \mathbb{R}^{a \times a}$ is the matrix of all ones and $I_a \in \mathbb{R}^{a \times a}$ is the identity matrix. Next suppose D is a $\{0, 1\}$ valued $a \times b$ dimensional matrix that has exactly d ones in each column. Finally let $\sigma = \sqrt{\delta(\delta - \eta^2 d)}/\eta$ and suppose the b -dimensional random vector \mathbf{Y} is given by*

$$\mathbf{Y} = D^t \mathbf{X} + \boldsymbol{\epsilon}$$

where $\boldsymbol{\epsilon}$ is another b -dimensional random vector independent of \mathbf{X} with $\text{Cov}(\boldsymbol{\epsilon}) = \sigma^2 I_b$. Then

$$\text{Cor}(\mathbf{X}, \mathbf{Y}) \odot D = \eta D \tag{11}$$

where $\text{Cor}(\mathbf{X}, \mathbf{Y}) \in \mathbb{R}^{a \times b}$ is the cross-correlation matrix between random vectors \mathbf{X} and \mathbf{Y} , and \odot represents the element-wise product of matrices (i.e., the Hadamard product).

Proof Since we are concerned with covariances, we can assume by mean centering that $\mathbf{E}\mathbf{X} = 0 \in \mathbb{R}^a$ and $\mathbf{E}\mathbf{Y} = \mathbf{E}\boldsymbol{\epsilon} = 0 \in \mathbb{R}^b$. Note that $D^t e_a = d e_b$ and $U_a = e_a e_a^t$, where $e_r \doteq (1, \dots, 1)^t \in \mathbb{R}^r$ for $r \in \{a, b\}$. Hence using independence of \mathbf{X} and $\boldsymbol{\epsilon}$:

$$\begin{aligned} \text{Cov}(\mathbf{Y}) &= \mathbf{E}(\mathbf{Y}\mathbf{Y}^t) = D^t \mathbf{E}(\mathbf{X}\mathbf{X}^t) D + \mathbf{E}(\boldsymbol{\epsilon}\boldsymbol{\epsilon}^t) \\ &= D^t \text{Cov}(\mathbf{X}) D + \text{Cov}(\boldsymbol{\epsilon}) = D^t (\rho e_a e_a^t + (1 - \rho) I_a) D + \sigma^2 I_b \\ &= \rho (D^t e_a)^t (D^t e_a) + (1 - \rho) D^t D + \sigma^2 I_b \\ &= \rho d^2 e_b e_b^t + (1 - \rho) D^t D + \sigma^2 I_b \end{aligned}$$

Since all the diagonal entries of $D^t D$ have the value d ,

$$\text{diag}[\text{Cov}(\mathbf{Y})] = (\rho d^2 + (1 - \rho)d + \sigma^2) I_b = (d\delta + \sigma^2) I_b = \left(\frac{\delta}{\eta}\right)^2 I_b \tag{12}$$

where for any square matrix A , $\text{diag}[A]$ denotes the diagonal matrix obtained from A by setting all the off-diagonal entries of A to 0.

We can similarly calculate the cross-covariance between \mathbf{X} and \mathbf{Y}

$$\begin{aligned} \text{Cov}(\mathbf{X}, \mathbf{Y}) &= \mathbf{E}(\mathbf{X}\mathbf{Y}^t) = \mathbf{E}(\mathbf{X}\mathbf{X}^t)D = (\rho e_a e_a^t + (1 - \rho)I_a)D \\ &= \rho d e_a e_b^t + (1 - \rho)D, \end{aligned} \tag{13}$$

and also finally the cross-correlation between \mathbf{X} and \mathbf{Y} using (13), (12) and $\text{diag}[\text{Cov}(\mathbf{X})] = I_a$:

$$\begin{aligned} \text{Cor}(\mathbf{X}, \mathbf{Y}) &= \text{diag}[\text{Cov}(\mathbf{X})]^{-\frac{1}{2}} \text{Cov}(\mathbf{X}, \mathbf{Y}) \text{diag}[\text{Cov}(\mathbf{Y})]^{-\frac{1}{2}} \\ &= \frac{\eta}{\delta} (\rho d e_a e_b^t + (1 - \rho)D) = \frac{\eta}{\delta} (\rho d \bar{D} + (1 - \rho + \rho d)D) \\ &= \eta D + \eta \rho d \delta^{-1} \bar{D}. \end{aligned}$$

where $\bar{D} \doteq 1 - D$. In particular this shows (11). ■

B.4.2 RESULTS FROM SCCA

As described in Section B.2, we ran sCCA on the simulated data to search for 100 canonical covariates for a range of values of the penalty parameter λ . The sizes of the bimodules for various values of λ can be seen in Figure 9. For $\lambda \in \{0.01, 0.02, 0.03, 0.04, .233\}$, the first two columns of the following table show the number of target bimodules (TB) that overlapped with each detected bimodule (DB) and the edge-error of each DB, both averaged over all DBs. The last column shows the top 5 (or bottom 95) percentile *recall* among the target bimodules.

λ	# TBs that overlap with each DB	edge-error	recall of TB (95%-tile)
.01	.97	.09	.02
.02	.96	.19	.23
.03	1.97	.48	.62
.04	6.47	.65	.95
.23	281	.89	1

The parameter value $\lambda = 0.01$ has small edge-error, but poor recall. The recall improves on increasing λ , but the edge-error degrades.

C. GTE_x results

C.1 Data acquisition and preprocessing

We obtained genotype and thyroid expression data for 574 individuals from the dbGap website (accession number: phs000424.v8.p1). We directly used the filtered and normalized gene expression data and covariates provided for eQTL analysis but filtered the SNPs in the genotype data using the LD pruning software *SNPRelate* Zheng (2015). The software retained 556K autosomal SNPs with minor allele frequency above 0.1 such that all pairs of SNPs within each 500KB window of the genome had squared correlation under $(0.7)^2$. The latter threshold was chosen to balance the number of retained SNPs and information loss. As SNPs exhibit local correlation due to linkage disequilibrium (LD), the selection process should not reduce the statistical power of BSP.

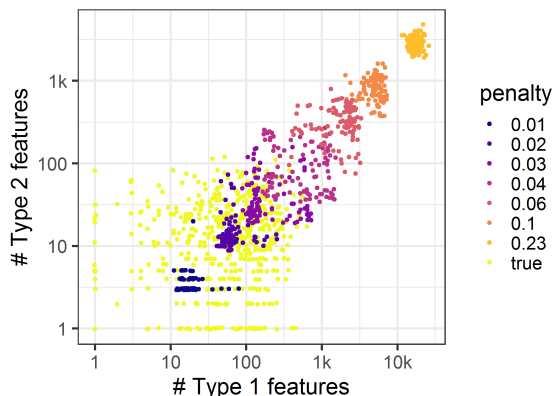


Figure 9: The sizes of sCCA bimodules for various values of the penalty parameter λ along with sizes of the target bimodules in yellow.

There were 68 covariates provided for the Thyroid tissue consisting of the top 5 genotype principle components; 60 PEER covariates, and 3 additional covariates for sequencing platform, sequencing protocol, and sex. We accounted for these covariates by the modification to BSP mentioned in Appendix A.4.

C.2 Running BSP

We applied BSP to the thyroid eQTL data with false discovery parameter $\alpha = 0.03$ selected to keep the edge-error estimates under 0.05 (details in Appendix C.4). The search was initialized from singleton sets of all genes and half of the available SNPs, chosen at random. Thus the search procedure in Section 2.4 was run $p/2 + q \sim 304\text{K}$ times. BSP took 4.7 hours to run on a computer with a 20-core 2.4 GHz processor (further processor details are provided in Appendix C.5). The search identified 3744 unique bimodules with p-values below the significance threshold of $\frac{\alpha}{pq} = 3.45 \times 10^{-12}$ (see Section 2.4). The majority (277K) of the searches terminated in the empty set after the first step; of the remaining 27K searches, the great majority identified a non-empty fixed point within 20 steps. Only 20 searches cycled and did not terminate in a fixed point. Among the searches taking more than one iteration, 94% terminated by the fifth step. Among searches that found a non-empty fixed point, 92.3% of the fixed points contained the seed singleton set of the search.

The effective number (see Section 2.5) of bimodules was 3304, slightly smaller than the number of unique bimodules. We applied the filtering procedure described in Section 2.5 to select from the unique bimodules a subfamily of 3304 bimodules that were substantially disjoint. The selected bimodules had SNP sets ranging in size from 1 to 1000, and gene sets ranging in size from 1 to 100 (Figure 3); the median size of the gene and SNP sets was 1 and 7, respectively.

If required, BSP can be run in a faster (less exhaustive) or slower (more exhaustive) fashion by selecting a smaller or larger fraction of SNPs from which to initialize the search procedure. The effective number of discovered bimodules was only slightly smaller (3258) when initializing with 10% of the SNPs.

C.3 Running Other Methods

Standard eQTL analysis was performed by applying Matrix-eQTL (Shabalin, 2012) twice to the data, first to perform a *cis*-eQTL analysis within a distance of 1MB and next to perform a *trans*-eQTL analysis. In each case, SNP-gene pairs with BH (Benjamini and Hochberg, 1995) q -value less than 0.05 were identified as significant. Matrix-eQTL identified 186K *cis*-eQTLs and 73K *trans*-eQTLs.

To obtain CONDOR bimodules (Platig et al., 2016), we applied Matrix-eQTL to identify both *cis*- and *trans*-eQTLs with BH q -value under the threshold .2, chosen as in Fagny et al. (2017). The resulting gene-SNP bipartite graph formed by these eQTLs was passed through CONDOR’s bipartite community detection pipeline (Platig et al., 2016), which partitioned the nodes of largest connected component of this graph into 6 bimodules.

We also applied the sCCA method of Witten et al. (2009) using the permutation based parameter selection procedure (Witten and Tibshirani, 2020) on the covariate-corrected genotype and expression matrices to identify 50 bimodules. The identified bimodules were large, containing roughly 100K SNPs and 4K-8K genes (Figure 3), making them difficult to analyze and interpret. The identified bimodules also exhibited moderate overlap: the effective number was 25. As such, we excluded the sCCA bimodules from subsequent comparisons. Analysis of sCCA on the simulated data (Section B.2.1) suggests that the method may be able to recover smaller bimodules with a more tailored choice of its parameters.

C.4 Choice of false discovery parameter to BSP

We chose the false discover parameter α for BSP from the grid $\{0.01, 0.02, 0.03, 0.04, 0.05\}$ by finding the largest α that kept the average edge-error estimates based on $N = 5$ half-permutations under 0.05 (see Appendix A.3). However our error estimates were variable as we obtained $\alpha = 0.05$ in one instance and $\alpha = 0.03$ in another. We conservatively chose $\alpha = 0.03$.

C.5 Hardware and software stack

The various methods used in this analysis were run on a dedicated computer that had Intel (R) Xeon (R) E5-2640 CPU with 20 parallel cores at 2.50 Hz base frequency, and a 512 GB random access memory along with L1, L2 and L3 caches of sizes 1.3, 5 and 50 MB respectively. The computer ran Windows server 2012 R2 operating system and we used the Microsoft R Open 3.5.3 software to perform most of our analysis, since it has multi-core implementations of linear algebra routines.

C.6 Bimodule connectivity thresholds and network sparsity

Figure 10 shows two network statistics for bimodules found by BSP – connectivity threshold and tree-multiplicity. All bimodules have tree multiplicity under 10. This shows that the association network for large bimodules, particularly having low connectivity-thresholds, is sparse.

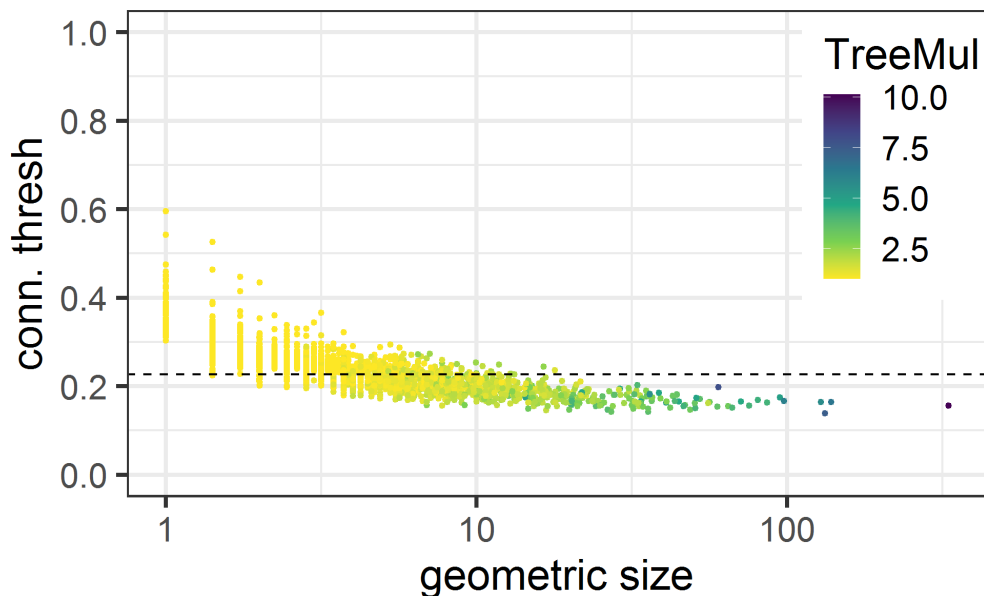


Figure 10: Connectivity-threshold and tree-multiplicity for BSP bimodules compared to their geometric size. The horizontal dotted line represents the threshold obtained from standard trans-analysis.

C.7 Connectivity of bimodules under edges from combined eQTL analysis

Here we examine which bimodules are connected under the combined edges from *cis*-eQTL and *trans*-eQTL analysis, based on geometric size of the bimodule. Figure 11 (left) shows that all the bimodules that have either one gene or one SNP are connected. Hence, these bimodules could have been recovered using standard eQTL analysis. On the other hand if we restrict to bimodules with two or more genes and SNPs, we see that (Figure 11; right) the fraction of connected bimodules tends to decrease as the geometric size of the bimodules increases.

C.8 Bimodule association networks

See the plots in Figure 12.

C.9 Gene Ontology

18 out of the 145 BSP gene sets, and 1 out of the 5 CONDOR gene sets that we considered had significant overlap with GO categories. Among the 40 GO terms detected by the CONDOR, 27 terms were also found among the 135 terms detected by BSP. The GO terms that were discovered for the two methods did not seem specific to thyroid, the tissue under investigation. Complete list of the GO terms for the two methods is as follows. Significant GO terms for BSP:

GO.ID	Term	bimod.
-------	------	--------

BIMODULE SEARCH PROCEDURE

1	GO:0060333	interferon-gamma-mediated signaling path...	1
2	GO:0002478	antigen processing and presentation of e...	1
3	GO:0019884	antigen processing and presentation of e...	1
4	GO:0048002	antigen processing and presentation of p...	1
5	GO:0019882	antigen processing and presentation	1
6	GO:0071346	cellular response to interferon-gamma	1
7	GO:0034341	response to interferon-gamma	1
8	GO:0019886	antigen processing and presentation of e...	1
9	GO:0002495	antigen processing and presentation of p...	1
10	GO:0002504	antigen processing and presentation of p...	1
11	GO:0045087	innate immune response	1
12	GO:0050776	regulation of immune response	1
13	GO:0006952	defense response	1
14	GO:0031295	T cell costimulation	1
15	GO:0031294	lymphocyte costimulation	1
16	GO:0050852	T cell receptor signaling pathway	1
17	GO:0002768	immune response-regulating cell surface ...	1
18	GO:0002764	immune response-regulating signaling pat...	1
19	GO:0050851	antigen receptor-mediated signaling path...	1
20	GO:0002682	regulation of immune system process	1
21	GO:0022409	positive regulation of cell-cell adhesio...	1
22	GO:0002253	activation of immune response	1
23	GO:0002429	immune response-activating cell surface ...	1
24	GO:0006950	response to stress	1
25	GO:0006955	immune response	1
26	GO:0019221	cytokine-mediated signaling pathway	1
27	GO:0002757	immune response-activating signal transd...	1
28	GO:0050870	positive regulation of T cell activation	1
29	GO:0002479	antigen processing and presentation of e...	1
30	GO:1903039	positive regulation of leukocyte cell-ce...	1
31	GO:0042590	antigen processing and presentation of e...	1
32	GO:0045806	negative regulation of endocytosis	2
33	GO:0050911	detection of chemical stimulus involved ...	3
34	GO:0007608	sensory perception of smell	3
35	GO:0050907	detection of chemical stimulus involved ...	3
36	GO:0009593	detection of chemical stimulus	3
37	GO:0007606	sensory perception of chemical stimulus	3
38	GO:0035459	cargo loading into vesicle	3
39	GO:0050906	detection of stimulus involved in sensor...	3
40	GO:0000038	very long-chain fatty acid metabolic pro...	4
41	GO:0006732	coenzyme metabolic process	4
42	GO:0006417	regulation of translation	5
43	GO:0034248	regulation of cellular amide metabolic p...	5
44	GO:0010608	posttranscriptional regulation of gene e...	5

45	GO:0046597	negative regulation of viral entry into ...	6
46	GO:0035455	response to interferon-alpha	6
47	GO:0035456	response to interferon-beta	6
48	GO:0046596	regulation of viral entry into host cell	6
49	GO:0045071	negative regulation of viral genome repl...	6
50	GO:1903901	negative regulation of viral life cycle	6
51	GO:0060337	type I interferon signaling pathway	6
52	GO:0071357	cellular response to type I interferon	6
53	GO:0034340	response to type I interferon	6
54	GO:0045069	regulation of viral genome replication	6
55	GO:0048525	negative regulation of viral process	6
56	GO:0019079	viral genome replication	6
57	GO:0046718	viral entry into host cell	6
58	GO:1903900	regulation of viral life cycle	6
59	GO:0030260	entry into host cell	6
60	GO:0044409	entry into host	6
61	GO:0051806	entry into cell of other organism involv...	6
62	GO:0051828	entry into other organism involved in sy...	6
63	GO:0043901	negative regulation of multi-organism pr...	6
64	GO:0034341	response to interferon-gamma	6
65	GO:0050792	regulation of viral process	6
66	GO:0051607	defense response to virus	6
67	GO:0051701	interaction with host	6
68	GO:0043903	regulation of symbiosis, encompassing mu...	6
69	GO:0009615	response to virus	6
70	GO:0051225	spindle assembly	7
71	GO:0007030	Golgi organization	7
72	GO:0007051	spindle organization	7
73	GO:0010256	endomembrane system organization	7
74	GO:0000226	microtubule cytoskeleton organization	7
75	GO:0007017	microtubule-based process	7
76	GO:0070925	organelle assembly	7
77	GO:0007010	cytoskeleton organization	7
78	GO:0007156	homophilic cell adhesion via plasma memb...	8
79	GO:0098742	cell-cell adhesion via plasma-membrane a...	8
80	GO:0098609	cell-cell adhesion	8
81	GO:0007155	cell adhesion	8
82	GO:0022610	biological adhesion	8
83	GO:0007416	synapse assembly	8
84	GO:0007267	cell-cell signaling	8
85	GO:0006355	regulation of transcription, DNA-templat...	9
86	GO:1903506	regulation of nucleic acid-templated tra...	9
87	GO:2001141	regulation of RNA biosynthetic process	9
88	GO:0006351	transcription, DNA-templated	9
89	GO:0097659	nucleic acid-templated transcription	9

BIMODULE SEARCH PROCEDURE

90	GO:0032774	RNA biosynthetic process	9
91	GO:0051252	regulation of RNA metabolic process	9
92	GO:2000112	regulation of cellular macromolecule bio...	9
93	GO:0010556	regulation of macromolecule biosynthetic...	9
94	GO:0019219	regulation of nucleobase-containing comp...	9
95	GO:0031326	regulation of cellular biosynthetic proc...	9
96	GO:0034654	nucleobase-containing compound biosynthe...	9
97	GO:0009889	regulation of biosynthetic process	9
98	GO:0018130	heterocycle biosynthetic process	9
99	GO:0019438	aromatic compound biosynthetic process	9
100	GO:0010468	regulation of gene expression	9
101	GO:1901362	organic cyclic compound biosynthetic pro...	9
102	GO:0016070	RNA metabolic process	9
103	GO:0001580	detection of chemical stimulus involved ...	10
104	GO:0050912	detection of chemical stimulus involved ...	10
105	GO:0050913	sensory perception of bitter taste	10
106	GO:0050909	sensory perception of taste	10
107	GO:0050907	detection of chemical stimulus involved ...	10
108	GO:0009593	detection of chemical stimulus	10
109	GO:0007606	sensory perception of chemical stimulus	10
110	GO:0050906	detection of stimulus involved in sensor...	10
111	GO:0007600	sensory perception	10
112	GO:0051606	detection of stimulus	10
113	GO:0050877	nervous system process	10
114	GO:0003008	system process	10
115	GO:0007186	G-protein coupled receptor signaling pat...	10
116	GO:0006355	regulation of transcription, DNA-templat...	11
117	GO:1903506	regulation of nucleic acid-templated tra...	11
118	GO:2001141	regulation of RNA biosynthetic process	11
119	GO:0006351	transcription, DNA-templated	11
120	GO:0097659	nucleic acid-templated transcription	11
121	GO:0032774	RNA biosynthetic process	11
122	GO:0051252	regulation of RNA metabolic process	11
123	GO:2000112	regulation of cellular macromolecule bio...	11
124	GO:0010556	regulation of macromolecule biosynthetic...	11
125	GO:0019219	regulation of nucleobase-containing comp...	11
126	GO:0031326	regulation of cellular biosynthetic proc...	11
127	GO:0034654	nucleobase-containing compound biosynthe...	11
128	GO:0009889	regulation of biosynthetic process	11
129	GO:0018130	heterocycle biosynthetic process	11
130	GO:0019438	aromatic compound biosynthetic process	11
131	GO:0010468	regulation of gene expression	11
132	GO:1901362	organic cyclic compound biosynthetic pro...	11
133	GO:0016070	RNA metabolic process	11
134	GO:1901685	glutathione derivative metabolic process	12

135	GO:1901687	glutathione derivative biosynthetic proc...	12
136	GO:0006749	glutathione metabolic process	12
137	GO:0042178	xenobiotic catabolic process	12
138	GO:0042537	benzene-containing compound metabolic pr...	12
139	GO:0006575	cellular modified amino acid metabolic p...	12
140	GO:0044272	sulfur compound biosynthetic process	12
141	GO:0046854	phosphatidylinositol phosphorylation	13
142	GO:0046834	lipid phosphorylation	13
143	GO:0048015	phosphatidylinositol-mediated signaling	13
144	GO:0048017	inositol lipid-mediated signaling	13
145	GO:0006882	cellular zinc ion homeostasis	14
146	GO:0055069	zinc ion homeostasis	14
147	GO:0010273	detoxification of copper ion	14
148	GO:1990169	stress response to copper ion	14
149	GO:0061687	detoxification of inorganic compound	14
150	GO:0097501	stress response to metal ion	14
151	GO:0071294	cellular response to zinc ion	14
152	GO:0071280	cellular response to copper ion	14
153	GO:0046916	cellular transition metal ion homeostasi...	14
154	GO:0071276	cellular response to cadmium ion	14
155	GO:0046688	response to copper ion	14
156	GO:0055076	transition metal ion homeostasis	14
157	GO:0072488	ammonium transmembrane transport	15
158	GO:0006089	lactate metabolic process	16
159	GO:0006882	cellular zinc ion homeostasis	17
160	GO:0055069	zinc ion homeostasis	17
161	GO:0006882	cellular zinc ion homeostasis	18
162	GO:0055069	zinc ion homeostasis	18

Significant GO terms for CONDOR

	GO.ID	Term	bimod
1	GO:0050852	T cell receptor signaling pathway	1
2	GO:0050851	antigen receptor-mediated signaling path...	1
3	GO:0006355	regulation of transcription, DNA-templat...	1
4	GO:1903506	regulation of nucleic acid-templated tra...	1
5	GO:2001141	regulation of RNA biosynthetic process	1
6	GO:0060333	interferon-gamma-mediated signaling path...	2
7	GO:0002478	antigen processing and presentation of e...	3
8	GO:0019884	antigen processing and presentation of e...	3
9	GO:0048002	antigen processing and presentation of p...	3
10	GO:0019886	antigen processing and presentation of e...	3
11	GO:0002495	antigen processing and presentation of p...	3
12	GO:0002504	antigen processing and presentation of p...	3
13	GO:0019882	antigen processing and presentation	3

BIMODULE SEARCH PROCEDURE

14	GO:0031295	T cell costimulation	3
15	GO:0031294	lymphocyte costimulation	3
16	GO:0060333	interferon-gamma-mediated signaling path...	3
17	GO:0050852	T cell receptor signaling pathway	3
18	GO:0050870	positive regulation of T cell activation	3
19	GO:1903039	positive regulation of leukocyte cell-ce...	3
20	GO:0050778	positive regulation of immune response	3
21	GO:0002253	activation of immune response	3
22	GO:0050851	antigen receptor-mediated signaling path...	3
23	GO:0022409	positive regulation of cell-cell adhesio...	3
24	GO:0071346	cellular response to interferon-gamma	3
25	GO:0051251	positive regulation of lymphocyte activa...	3
26	GO:1903037	regulation of leukocyte cell-cell adhesi...	3
27	GO:0034341	response to interferon-gamma	3
28	GO:0002696	positive regulation of leukocyte activat...	3
29	GO:0050863	regulation of T cell activation	3
30	GO:0050867	positive regulation of cell activation	3
31	GO:0007159	leukocyte cell-cell adhesion	3
32	GO:0050776	regulation of immune response	3
33	GO:0002429	immune response-activating cell surface ...	3
34	GO:0002684	positive regulation of immune system pro...	3
35	GO:0006955	immune response	3
36	GO:0022407	regulation of cell-cell adhesion	3
37	GO:0045087	innate immune response	3
38	GO:0002768	immune response-regulating cell surface ...	3
39	GO:0045785	positive regulation of cell adhesion	3
40	GO:0002455	humoral immune response mediated by circ...	3
41	GO:0051249	regulation of lymphocyte activation	3
42	GO:0019221	cytokine-mediated signaling pathway	3
43	GO:0042110	T cell activation	3

D. Climate analysis details

Figure 13 shows the edge-error estimates we used to choose α . Table 4 shows a summary of cross-correlations for each precipitation pixel from the two BSP bimodules.

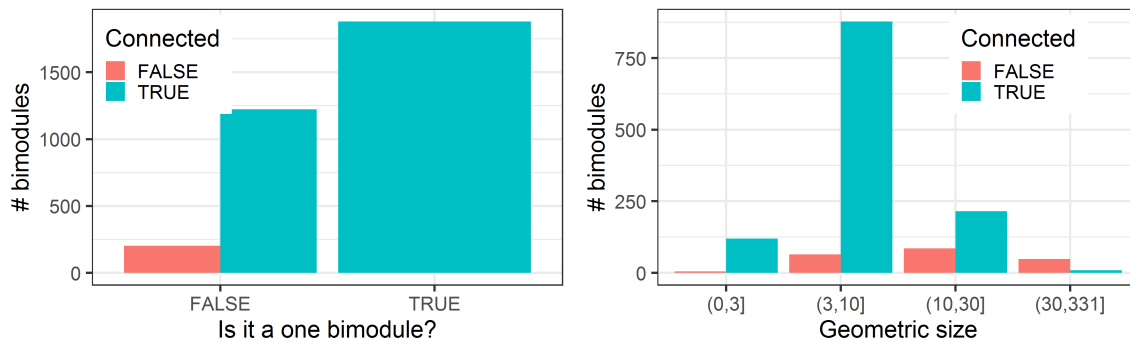


Figure 11: Connectivity of BSP bimodules under combined edges from *cis*-eQTL and *trans*-eQTL analysis. Left: the number of bimodules that are connected and are *one bimodules* (i.e. have one gene or one SNP). Right: Among bimodules having two or more genes and SNPs (i.e. are not one bimodules), the connectivity and geometric size of the bimodules.

	P Pixel	Mean	SD
A	1	0.28	0.07
	2	0.27	0.06
	3	0.28	0.08
	4	0.27	0.08
	5	0.31	0.06
	6	0.30	0.08
	P Pixel	Mean	SD
B	1	0.31	0.04
	2	0.35	0.03
	3	0.29	0.04

Table 4: Summary of the cross-correlations for each precipitation (P) pixel in the two BSP bimodules A and B from the climate data. Each entry shows the mean and standard deviation of the cross-correlations of each P in the bimodule with other T pixels in the same bimodule. Results show that all of the cross-correlations tend to be strong and positive.

BIMODULE SEARCH PROCEDURE

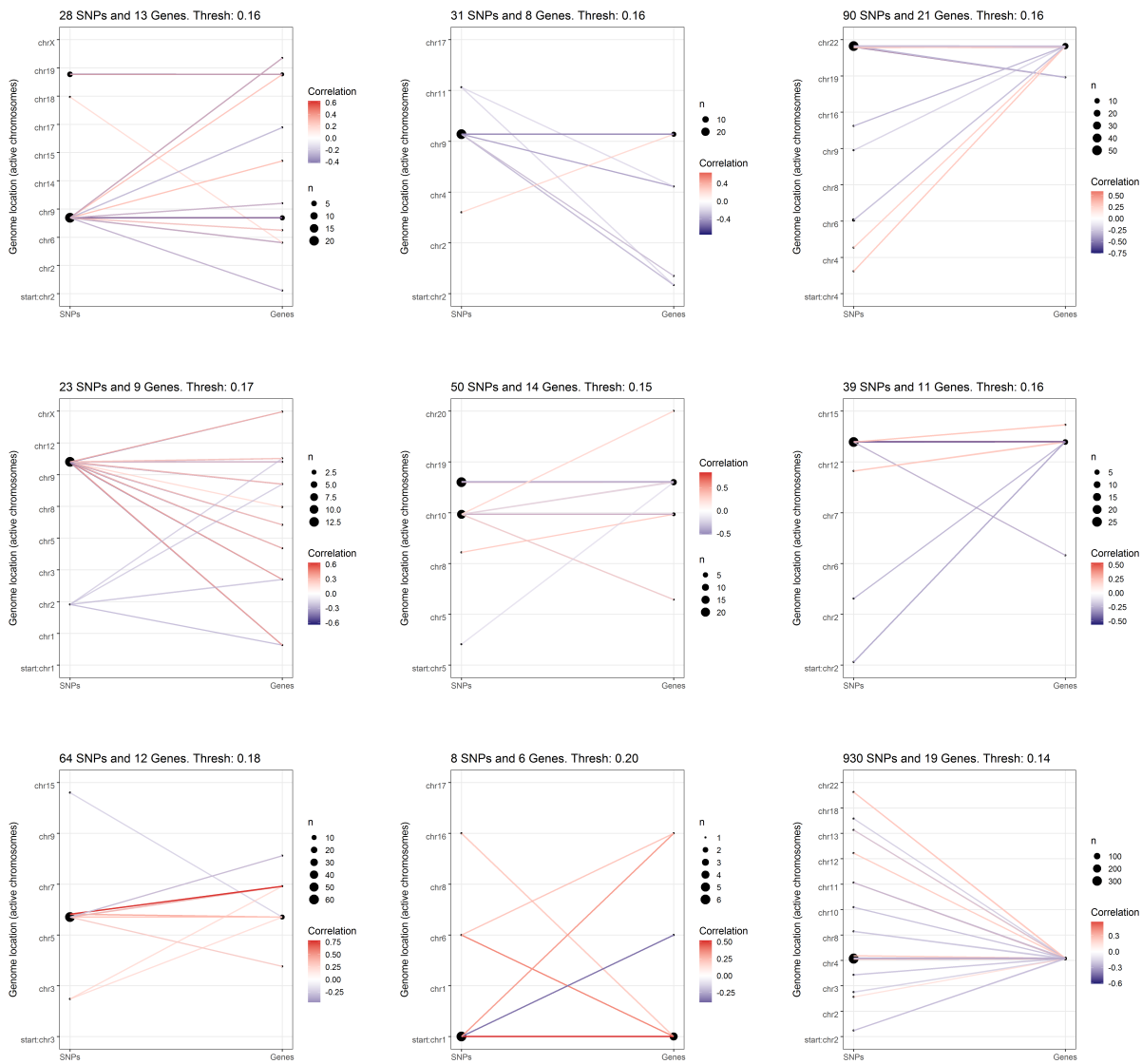


Figure 12: Out of 31 BSP bimodules that had genes on 3 or more chromosomes and SNPs on 2 or more chromosomes, we selected 9 bimodules that looked interesting. The bipartite graph for each bimodule is formed out of the essential edges (Section 4.2.3).

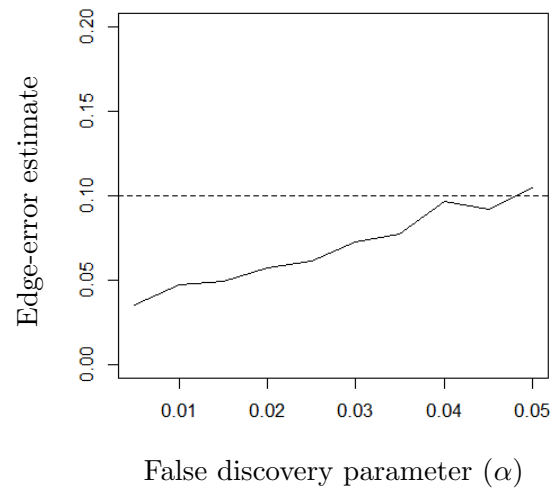


Figure 13: Average edge-error estimates for BSP results for the climate data based on 100 half-permutations (Section A.3.1) for α ranging from 0.01 to 0.05. The edge-error estimates exceed 0.05 for the first time at $\alpha = 0.045$.